## Updated constraints from the effective field theory analysis of the BOSS power spectrum on early dark energy

Théo Simon<sup>®</sup>, <sup>1,\*</sup> Pierre Zhang<sup>®</sup>, <sup>2,†</sup> Vivian Poulin<sup>®</sup>, <sup>1</sup> and Tristan L. Smith<sup>3</sup>

<sup>1</sup>Laboratoire Univers et Particules de Montpellier (LUPM),

CNRS et Université de Montpellier (UMR-5299), Place Eugène Bataillon,

F-34095 Montpellier Cedex 05, France

Department of Astronomy, School of Physical Sciences, University of Science and Technology

<sup>2</sup>Department of Astronomy, School of Physical Sciences, University of Science and Technology of China, Hefei, Anhui 230026, China;

CAS Key Laboratory for Research in Galaxies and Cosmology, University of Science and Technology of China, Hefei, Anhui 230026, China; and School of Astronomy and Space Science, University of Science and Technology of China, Hefei, Anhui 230026, China

<sup>3</sup>Department of Physics and Astronomy, Swarthmore College, Swarthmore, Pennsylvania 19081, USA

(Received 29 August 2022; accepted 30 January 2023; published 3 March 2023)

Analyses of the full shape of the Baryon Oscillation Spectroscopic Survey (BOSS) DR12 power spectrum using the one-loop prediction from the effective field theory of large-scale structures (EFTBOSS) have led to new constraints on extensions to the  $\Lambda$  cold dark matter model, such as early dark energy (EDE), which has been suggested as a resolution to the "Hubble tension." In this paper, we reassess the constraining power of the EFTBOSS on EDE in light of a correction to the normalization of BOSS window functions. Overall we find that constraints from EFTBOSS on EDE are weakened and represent a small change compared to constraints from Planck and the conventional baryon acoustic oscillation/ $f\sigma_8$ measurements. The combination of Planck data with EFTBOSS provides a bound on the maximal fractional contribution of EDE  $f_{\rm EDE} < 0.083$  at 95% C.L. (compared to <0.054 with the incorrect normalization and <0.088 without full-shape data) and the Hubble tension is reduced to  $2.1\sigma$ . However, the more extreme model favored by an analysis with just data from the Atacama Cosmology Telescope is disfavored by the EFTBOSS data. We also show that the updated Pantheon + type Ia supernova (SN1a) analysis can slightly increase the constraints on EDE. Yet, the inclusion of the SN1a magnitude calibration by SH0ES strongly increases the preference for EDE to above  $5\sigma$ , yielding  $f_{\rm EDE} \sim 0.12^{+0.03}_{-0.02}$  around the redshift  $z_c = 4365^{+3000}_{-1100}$ . Our results demonstrate that EFTBOSS data (alone or combined with Planck data) do not exclude the EDE resolution of the Hubble tension.

#### DOI: 10.1103/PhysRevD.107.063505

#### I. INTRODUCTION

In recent years, several tensions between probes of the early and late Universe analyzed under the  $\Lambda$  cold dark matter model ( $\Lambda$ CDM) have emerged. The Hubble tension refers to the inconsistency between local measurements of the current expansion rate of the Universe, i.e., the Hubble constant  $H_0$ , and the value inferred from early Universe data using the  $\Lambda$ CDM model. This tension is predominantly driven by the Planck Collaboration's observation of the cosmic microwave background (CMB), which predicts a value in  $\Lambda$ CDM of  $H_0 = 67.27 \pm 0.60$  km/s/Mpc [1], and the value measured by the SH0ES Collaboration using the Cepheid-calibrated cosmic distance ladder, whose latest

measurement yields  $H_0 = 73 \pm 1$  km/s/Mpc [2,3]. Taken at face value, these observations alone result in a ~5 $\sigma$  tension. Experimental efforts are underway to establish whether this discrepancy can be caused by yet unknown systematic effects (appearing in either the early or late Universe measurements [4,5], or both). It appears that various attempts to alter the modeling of dust extinction are not successful in altering the Hubble constant [6–8], nor is there support for different populations of type Ia supernova (SNIa) at low z and high z causing significant impact [9–12]. In fact, the SH0ES team recently provided a comprehensive measurement of the  $H_0$  parameter to 1.3% precision, addressing these potential systematic errors, and concluded that there is "no indication that the discrepancy

theo.simon@umontpellier.fr pierrexyz@protonmail.com

<sup>&</sup>lt;sup>1</sup>A new calibration including cluster Cepheids and Gaia EDR3 parallaxes further increase the tension to  $5.3\sigma$  [3].

arises from measurement uncertainties or [over 70] analysis variations considered to date" [2]. On the side of the CMB, it has been noted that Planck data carry a number of anomalies of low statistical significance that may play a role in this tension [1,13–16]. Nevertheless, the appearance of this discrepancy across an array of probes<sup>2</sup> (although not always with strong statistical significance) suggests that a single systematic effect may not be sufficient to resolve it. For recent reviews on the topic, we refer the reader to Refs. [31,32].

Additionally, within  $\Lambda$ CDM, the parameter  $S_8 \equiv$  $\sigma_8(\Omega_m/0.3)^{0.5}$ , where  $\sigma_8$  is the root mean square of matter fluctuations on an  $8h^{-1}$  Mpc scale and  $\Omega_m$  the (fractional) matter density today, inferred from CMB is about  $2-3\sigma$ larger than that deduced from weak lensing surveys such as the CFHTLenS [33], KiDS-1000 [34], DESY3 [35], as well as from Planck Sunyaev-Zeldovich cluster abundances [1,36] and SPT [37]. Additionally, the measurements of  $S_8$  on large scales with galaxy clustering from Baryon Oscillation Spectroscopic Survey (BOSS) full-shape data that have been reported also indicate a value that is on a low side, although not at an important significant level due to large error bars ( $\sim 2\sigma$ ) [38,39].<sup>3</sup> It is yet to be understood whether the  $S_8$  tension is due to systematic effects [42], nonlinear modeling, including the effect of baryons at very small scales [41], or physics beyond  $\Lambda$ CDM.

Along with experimental developments to confirm the Hubble and  $S_8$  tension, a lot of effort has been given to

<sup>3</sup>Note that, however, these  $S_8$  measurements might be affected by prior volume effects, as shown and quantified in [40]. Once those are accounted for, BOSS full-shape results and Planck are brought to good agreement (see also [41]).

explain these discrepancies with some new physical mechanism, often in the form of extensions to the  $\Lambda$ CDM model that may be connected to the (still unknown) nature of dark matter or dark energy. It has been argued that the most promising category of solutions to resolve the  $H_0$  tension involves physics in the prerecombination era leading to a decrease of the sound horizon at recombination [43–48], such as models involving dark radiation and/or new neutrino properties [49–59], early dark energy (EDE) [60–65], modified gravity [66–85], or exotic recombination [86–90] (for reviews, see Refs. [31,48]).

Interestingly, these models tend to leave signatures in the matter power spectrum on large scales that can be probed by large-scale structure surveys such as SDSS/ BOSS [91]. In fact, developments of the one-loop prediction of the galaxy power spectrum in redshift space from the effective field theory of large-scale structures (EFTofLSS)<sup>4</sup> [92–97] have made possible the determination of the  $\Lambda$ CDM parameters from the full-shape analysis of SDSS/BOSS data [91] at precision higher than that from conventional BAO and redshift space distortions (which measure the product  $f\sigma_8$ , where f is the growth function) analyses, and even comparable to that of CMB experiments. This provides an important consistency test for the ACDM model, while allowing one to derive competitive constraints on models beyond ACDM (see, e.g., Refs. [38,39,98–107]). A thorough study of the consistency of EFTBOSS analyses within the ΛCDM model is presented in a companion paper [108].

In this paper, we reassess the constraints on EDE from the full shape of the most recent measurements of the power spectrum (or correlation function) of BOSS in light of a correction to the normalization of BOSS window functions (presented in Appendix A). EDE has been shown to reduce the Hubble tension to the  $\sim 1.5\sigma$  level, with an energy density representing at most a fraction  $f_{\rm EDE}(z_c) \sim 12\%$  at the critical redshift  $z_c \sim 3500$  after which the fields start to dilute away [48,60–62]. There exists a variety of other EDE models that can similarly reduce the tension to the  $1.5-2.5\sigma$ level [63,65,109–111]. Recently, several groups have reported "hints" of EDE within ACT data at the  $\sim 3\sigma$  level, alone or in combination with WMAP (or, equivalently, Planck temperature data restricted to  $\ell < 650$ ) and Planck polarization data [112,113], as well as with SPT-3G data [114,115].

However, it has also been pointed out that EDE leaves an impact in the matter power spectrum that can be constrained thanks to the EFTofLSS applied to BOSS data or through measurements of the parameter  $S_8$ . Typically, in the EDE cosmology that resolves the Hubble tension, the amplitude of fluctuations  $\sigma_8$  is slightly larger due to increase in  $\omega_{\rm cdm}$ 

<sup>&</sup>lt;sup>2</sup>For a very short summary of alternative methods, let us mention that, on the one hand, there exists a variety of different techniques for calibrating ΛCDM at high redshifts and subsequently inferring the value of  $H_0$ , which do not involve Planck data. For instance, one can use alternative CMB datasets such as Wilkinson Microwave Anisotropy Probe (WMAP), ACT, or SPT, or even remove observations of the CMB altogether and combine measurements of big bang nucleosynthesis (BBN) with data from baryon acoustic oscillation (BAO) [17,18], resulting in  $H_0$  values in good agreement with Planck. On the other hand, alternative methods for measuring the local expansion rate have been proposed in the literature, in an attempt at removing any bias introduced from Cepheid and/or SNIa observations. The Chicago-Carnegie Hubble program (CCHP), which calibrates SNIa using the tip of the red giant branch (TRGB), obtained a value of  $H_0 =$  $69.8 \pm 0.6 (\text{stat}) \pm 1.6 (\text{sys}) \text{ km/s/Mpc}$  [19,20], in between the Planck CMB prediction and the SH0ES calibration measurement, and a reanalysis of the CCHP data by Anand et al. yields  $H_0 =$  $71.5 \pm 1.9 \text{ km/s/Mpc}$  [21]. The SH0ES team, using the parallax measurement of  $\omega$ -Centauri from Gaia DR3 to calibrate the TRGB, obtained  $H_0 = 72.1 \pm 2.0 \text{ km/s/Mpc}$  [22,23]. Additional methods intended to calibrate SNIa at large distances include surface brightness fluctuations of galaxies [24], Miras [25], or the Baryonic Tully Fisher relation [26]. There also exists a variety of observations that do not rely on observations of SNIa—these include, e.g., time delay of strongly lensed quasars [27,28], maser distances [29], or gravitational waves as "standard sirens" [30].

<sup>&</sup>lt;sup>4</sup>See also the introduction footnote in, e.g., [40] for relevant related works on the effective field theory of large-scale structures (EFTofLSS).

and  $n_s$ , which are necessary to counteract some of the effects of the EDE on the CMB power spectra [61,116,117]. As a result, the  $S_8$  tension tends to increase by  $\sim 0.5\sigma$  in the EDE cosmology, and large-scale structure (LSS) measurements may put pressure on the EDE model [116]. Additionally, it has been argued that the full-shape analysis of the galaxy power spectrum of BOSS disfavors the EDE model as an efficient resolution of the  $H_0$  tension [118,119]. Indeed, in order to adjust the BAO data seen either in 3D or 2D at different comoving distances in a galaxy clustering survey (typically at  $z \sim 0.1-1$ ), it requires in the EDE cosmology an increase in  $\omega_{\rm cdm}^{5}$  [61,89], which can affect the fit to the full shape [116,118,119]. Thus, galaxy clustering data can provide a way to break the degeneracy introduced by EDE, in particular, due to the constraints it provides on  $\omega_{\rm cdm}$  and  $\sigma_8$ .

Although these effects are certainly relevant in constraining EDE, the original interpretation of the additional constraining power suggested in Refs. [118,119] was disputed in Refs. [120,121]. There, it was argued that the apparent constraining power from the BOSS full-shape analysis may be artificially amplified by (i) the impact of the prior volume artificially favoring  $\Lambda$ CDM in the Bayesian context (later verified with a profile likelihood approach [123,124]); (ii) a potential ~20% mismatch in the overall amplitude (typically parametrized by the primordial power spectrum amplitude  $A_s$ ) between BOSS and Planck, rather than additional constraints on  $\omega_{\rm cdm}$ . In parallel, it had already been pointed out in Ref. [125] that the effective field theory of LSS applied to BOSS data does not rule out the new EDE model.

In Appendix A, we explore the impact of the correction to the normalization of the BOSS data window function within  $\Lambda$ CDM and show that it leads to a  $1\sigma$  shift upward in the value of  $A_s$ , now in better agreement with Planck. Given that previous analyses, e.g., Refs. [118,119], have used the measurements inconsistently normalized between the power spectrum and the window function (as already acknowledged in Ref. [126] for their previous analyses), the constraints from EDE are expected to change with these corrected BOSS measurements. While Refs. [118,119] concluded that the BOSS data, combined with Planck data, disfavored the EDE model as a potential candidate to solve the  $H_0$  tension, we find here that the conclusions reached strongly depend on the normalization of the window functions used in the BOSS measurements.

Our paper is structured as follows: In Sec. II, we review the EDE model and data considered in this work. In particular, we detail the possible choice of BOSS measurements and EFT likelihoods. In Sec. III, we assess the constraining power of corrected BOSS data alone on the EDE resolution to the Hubble tension and discuss differences between the constraints derived from the various BOSS data and effective field theory likelihoods. In Sec. IV, we derive constraints on EDE from the EFTBOSS data combined with either Planck data (with and without SH0ES) or ACT data. We also show the impact of the new Pantheon+ SN1a catalog [127] on the constraints on EDE. We eventually present our conclusions in Sec. V. Appendix A presents details on how to consistently normalize the window function with the power spectrum measurements. Appendix B provides additional comparison between EFTofLSS likelihoods within the EDE model. Finally, Appendix C lists additional relevant information about  $\chi^2$  statistics.

#### II. EARLY DARK ENERGY MODEL AND DATA

#### A. Brief review of the model

The EDE model corresponds to an extension of the  $\Lambda$ CDM model, where the existence of an additional subdominant oscillating scalar field  $\phi$  is considered. The EDE field dynamics is described by the Klein-Gordon equation of motion (at the homogenous level),

$$\ddot{\phi} + 3H\dot{\phi} + V_{n,\phi}(\phi) = 0, \tag{1}$$

where  $V_n(\phi)$  is a modified axion-like potential defined as

$$V_n(\phi) = m^2 f^2 [1 - \cos(\phi/f)]^n. \tag{2}$$

f and m correspond to the decay constant and the effective mass of the scalar field, respectively, while the parameter n controls the rate of dilution after the field becomes dynamical. In the following, we will use the redefined field quantity  $\Theta = \phi/f$  for convenience, such that  $-\pi \leq \Theta \leq +\pi$ .

At early times, when  $H\gg m$ , the scalar field  $\phi$  is frozen at its initial value since the Hubble friction prevails, which implies that the EDE behaves like a form of dark energy and that its contribution to the total energy density increases relative to the other components. When the Hubble parameter drops below a critical value  $(H\sim m)$ , the field starts evolving toward the minimum of the potential and becomes dynamical. The EDE contribution to the total budget of the Universe is maximum around a critical redshift  $z_c$ , after which the energy density starts to dilute with an approximate equation of state  $w_{\phi}=P_{\phi}/\rho_{\phi}$  [128,129],

<sup>&</sup>lt;sup>5</sup>A similar increase is required to keep the CMB peaks height fixed [61], in particular, through the Integrated Sachs-Wolfe (ISW) effect [117].

<sup>&</sup>lt;sup>6</sup>For further discussion about the mitigation of projection and prior volume effect, see Ref. [122].

<sup>&</sup>lt;sup>7</sup>Note that, in our companion paper [108], we argue that the remaining difference on the amplitude might be explained by projection effects from the prior volume associated with the marginalization of the EFT parameters.

$$w_{\phi} = \begin{cases} -1 & \text{if } z > z_c, \\ \frac{n-1}{n+1} & \text{if } z < z_c. \end{cases}$$
 (3)

In the following, we will fix n=3 as it was found that the data are relatively insensitive to this parameter provided  $2 \lesssim n \lesssim 5$  [62]. Instead of the theory parameters f and m, we make use of  $f_{\rm EDE}(z_c)$  and  $z_c$  determined through a shooting method [62]. We also include the initial field value  $\Theta_i$  as a free parameter, whose main role once  $f_{\rm EDE}(z_c)$  and  $z_c$  are fixed is to set the dynamics of perturbations right around  $z_c$ , through the EDE sound speed  $c_s^2$ .

The EDE field will provide a small contribution to the expansion rate H(z) around  $z_c$  (we will focus on  $\sim 10^3 - 10^4$  in the context of the Hubble tension), which causes a modification of the sound horizon at the recombination

$$r_{\rm s}(z_{\rm rec}) = \int_{z_{\rm rec}}^{+\infty} \frac{c_{\rm s}(z')}{H(z')} dz', \tag{4}$$

where  $c_s$  corresponds to the sound speed of the photonbaryon fluid acoustic waves. The sound horizon is observationally determined through the angular acoustic scale at recombination  $\theta_s$ , defined as

$$\theta_s = \frac{r_s(z_{\text{rec}})}{D_A(z_{\text{rec}})},\tag{5}$$

where  $D_A(z_{\rm rec}) = \int_0^{z_{\rm rec}} dz'/H(z') \propto 1/H_0$  is the comoving angular diameter distance. Given that  $\theta_s$  is determined from Planck CMB power spectra with a very high accuracy, the change in the sound horizon must be compensated by a readjustment of the angular diameter distance in order to keep the angular acoustic scale constant. This readjustment is automatically done by increasing  $H_0$  (and additional shift in  $\omega_{\rm cdm}$  and  $n_s$  to compensate effect of EDE on the growth of perturbations), which can, by design, bring the CMB measurements and the late-time estimate of the Hubble constant from the SH0ES Collaboration into agreement. In this paper, we address the question of whether the current full shape of galaxy clustering data analyzed using the EFTofLSS, can accommodate EDE. Indeed, on the one hand, the sound horizon seen at baryon-drag epoch  $r_s(z_{\text{drag}})$ is measured through another angular acoustic scale in galaxy surveys,

$$\theta_g = \frac{r_s(z_{\text{drag}})}{D_V(z_{\text{eff}})},\tag{6}$$

where  $z_{\rm eff}$  is the effective redshift of the survey, and  $D_V(z)=(D_A^2(z)\frac{c\cdot z}{H(z)})^{1/3}$  is a volume average of the comoving distances in the directions parallel and perpendicular to the line of sight, with c the speed of light. The angle  $\theta_g$  typically summarizes the information from the BAO, and measuring it with high precision has the potential to break

the degeneracy between  $r_s(z_{\text{drag}})$  and  $H_0$  introduced by the EDE. In practice, BAOs from BOSS were shown to be well fit in combination with Planck and SH0ES when allowing for EDE [61], at the cost of a larger  $\omega_{\rm cdm}$  [130], which can simultaneously allow for the CMB peak height to be kept fixed [61] through the ISW effect [117]. However, the fullshape of the galaxy power spectrum also contains additional information. For example, the amplitude of the small-scale galaxy power spectrum at  $k > k_{eq}$ , where  $k_{eq}$ is the wavenumber entering the horizon at matter/radiation equality, contains information about  $\omega_m$ , h, and the spectral tilt  $n_s$  [98,100]. As the values of  $\omega_{\rm cdm}$  and  $n_s$  are uplifted to compensate the growth of perturbations in the presence of EDE, the full shape of the galaxy power spectrum (with  $\omega_b$ fixed by CMB or a BBN prior) is also modified in that respect. In the following, we quantify if these modifications from the EDE as a resolution of the  $H_0$  tension are consistent with current cosmological data, including the full-shape galaxy power spectrum from BOSS modeled with the EFT.

#### B. Data and method

We analyze the EDE model in light of recent cosmological observations through a series of Markov chain Monte Carlo (MCMC) analyses using the Metropolis-Hastings algorithm from MONTE PYTHON v3<sup>8</sup> code [131,132] interfaced with our modified version of CLASS<sup>10</sup> [133]. In this paper, we carry out various analyses from a combination of the following datasets:

- (i) PlanckTTTEEE: The low-*l* CMB TT, EE, and the high-*l* TT, TE, EE data from Planck 2018 [1].
- (ii) PlanckTT650TEEE: Same dataset as Planck TTTEEE, but in this case the TT power spectrum has a multipole range restricted to l < 650.
- (iii) Lens: The CMB gravitational lensing potential reconstructed from Planck 2018 temperature and polarization data [134]. When used without high-*l* TT, TE, EE data, we use the CMB-marginalized version of the likelihood.<sup>11</sup>
- (iv) ACT: The temperature and polarization angular power spectrum of the CMB from the Atacama Cosmology Telescope (ACT DR4) [135].
- (v) BBN: The BBN measurement of  $\omega_b$  [136] that uses the theoretical prediction of [137], the experimental deuterium fraction of [138], and the experimental helium fraction of [139].
- (vi) BAO: The measurements of the BAO from the CMASS and LOWZ galaxy samples of BOSS DR12 at  $z=0.38,\ 0.51,\$ and  $0.61\$ [91], which we

<sup>&</sup>lt;sup>8</sup>https://github.com/brinckmann/montepython\_public.

https://github.com/PoulinV/AxiCLASS.

https://lesgourg.github.io/class\_public/class.html.

<sup>&</sup>lt;sup>11</sup>We thank Oliver Philcox for his help with correcting a bug in the standard Plik implementation.

TABLE I. Comparison of pre- and post-reconstructed BOSS two-point function measurements: reference, estimator, code of the measurements, redshift split [LOWZ, 0.2 < z < 0.43 ( $z_{\text{eff}} = 0.32$ ); CMASS, 0.43 < z < 0.7 ( $z_{\text{eff}} = 0.57$ );  $z_1$ , 0.2 < z < 0.5 $(z_{\rm eff} = 0.38); z_3, 0.5 < z < 0.7 (z_{\rm eff} = 0.61)],$  and window function treatment. For the post-reconstructed measurements, while we instead provide under "Method" the references presenting the algorithm used to extract the reconstructed BAO parameters and how the cross-correlation with the pre-reconstructed measurements is performed, "Ref." now refers to the public post-reconstructed measurements used. The SDSS-III BOSS DR12 galaxy sample data are described in Refs. [91,143]. The pre-reconstructed measurements are from BOSS catalogs DR12 (v5) combined CMASS-LOWZ<sup>g</sup> [144]. More details can be found in Sec. IV of Ref. [108].

	Pre-reconstructed measurements									
	Reference	Estimator	Code	Redshift split	Window					
$\mathcal{P}_{FKP}^{LZ/CM}$	[147]	FKP	RUSTICO <sup>a</sup> [147]	LOWZ/CMASS	Inconsistent normalization					
$P_{ m FKP}^{ m LZ/CM}$	[38]	FKP	Powspec <sup>b</sup> [148]/NBODYKIT <sup>c</sup> [149]	LOWZ/CMASS	Consistent normalization					
ξLZ/CM	[38]	Landy and Slazay	FCFC <sup>d</sup> [148]	LOWZ/CMASS	Window-free					
$P_{ m FKP}^{z_1/z_3}$	[150] <sup>e</sup>	FKP	• • •	$z_1/z_3$	Consistent normalization					
$P_{ m QUAD}^{z_1/z_3}$	[39]	Quadratic	SPECTRA WITHOUT WINDOWS <sup>f</sup> [151]	$z_1/z_3$	Window-free					
QUID			Post-reconstructed measurements							
	Reference	•••	•••	Redshift split	Method					
$lpha_{ m rec}^{ m LZ/CM}$	[142]	•••	• • •	LOWZ/CMASS	[101]					
$lpha_{ m rec}^{z_1/z_3}$	[152]	• • •	• • •	$z_1/z_3$	[101]					
$\beta_{\rm rec}^{z_1/z_3}$	[152]		•••	$z_1/z_3$	[153]					

ahttps://github.com/hectorgil/Rustico.

refer to as BOSS BAO DR12, and the BAO measurements from 6DF galaxy survey (6dFGS) at z = 0.106 and SDSS DR7 at z = 0.15 [140,141], which we refer to as BOSS BAO low z.

- (vii) BOSS  $f\sigma_8$  DR12: We also sometimes include the redshift space distortion at z = 0.38, 0.51, and 0.61, which we refer to as  $f\sigma_8$  [91], taking into account the cross-correlation with BAO measurements.
- (viii) EFTBOSS: The full-shape analysis BOSS power spectrum from the EFTofLSS, namely,  $P_{\text{FKP}}^{\text{LZ/CM}}$  [38], cross-correlated with reconstructed BAO, namely,  $\alpha_{\text{rec}}^{\text{LZ/CM}}$  [142]. The measurements are defined in Table I. The SDSS-III BOSS DR12 galaxy sample data and covariances are described in Refs. [91,143]. The measurements, obtained in Ref. [38], are from BOSS catalogs DR12 (v5) combined CMASS-LOWZ<sup>12</sup> [144] and are divided in redshift bins LOWZ 0.2 < z < 0.43 ( $z_{\text{eff}} = 0.32$ ) and CMASS 0.43 < z < 0.7 ( $z_{\text{eff}} = 0.57$ ), with north and south Galactic skies for each, respectively, denoted NGC and SGC. For the EDE analyses, we analyze the full shape of CMASS NGC, CMASS SGC, and LOWZ NGC, cross-correlated with postreconstruction BAOs. The analysis includes the

- (ix) Pan18: The Pantheon SNIa catalog, spanning redshifts 0.01 < z < 2.3 [145]. We will also study in Sec. IV D the impact of the newer Pantheon + catalog, favoring a larger  $\Omega_m$  [127], on our conclusions.
- (x) SH0ES: The SH0ES determination of  $H_0 =$  $73.04 \pm 1.04 \text{ km/s/Mpc}$  from Cepheid-calibrated SNIa, modeled as a Gaussian likelihood.<sup>13</sup>

We will refer to the combination of Planck TTTEEE + BAO + Pan18 as BaseTTTEEE, and to BaseTT650TEEE

https://github.com/cheng-zhao/powspec.

chttps://github.com/bccp/nbodykit.dhttps://github.com/cheng-zhao/FCFC.

ehttps://fbeutler.github.io/hub/deconv\_paper.html.

https://github.com/oliverphilcox/Spectra-Without-Windows.

ghttps://data.sdss.org/sas/dr12/boss/lss/.

monopole and quadrupole between  $(k_{\min}, k_{\max}) =$  $(0.01, 0.20/0.23)h \text{ Mpc}^{-1}$  in Fourier space and  $(s_{\min}, s_{\max}) = (25/20, 200) \text{ Mpc/}h \text{ in configuration}$ space [38,100,101] for LOWZ/CMASS. The theory prediction and likelihood are made available through PyBird. We also compare PyBird to CLASS-PT. More details on the differences between these likelihoods are given in Sec. II of Ref. [108]. When computing constraints with CLASS-PT, we use the galaxy power spectrum monopole, quadrupole, and hexadecapole, for  $0.01 \le k \le 0.2h \text{ Mpc}^{-1}$  as well as the real-space extension  $Q_0$ , up to  $k_{\text{max}} = 0.4h \text{ Mpc}^{-1}$ , and the post-reconstructed BAO parameters. We use the standard CLASS-PT priors on the bias parameters.

<sup>&</sup>lt;sup>12</sup>https://data.sdss.org/sas/dr12/boss/lss/.

<sup>&</sup>lt;sup>13</sup>For discussions about this modeling, see Refs. [46–48].

when replacing Planck TTTEEE with Planck TT650TEEE. In the absence of CMB TTTEEE data, we refer to the dataset EFTBOSS + BBN + Lens + BAO + Pan 18as BaseEFTBOSS. For all runs performed, we use Planck conventions for the treatment of neutrinos, that is, we include two massless and one massive species with  $m_{\nu} = 0.06$  eV [1]. In addition, we impose a large flat prior on the dimensionless baryon energy density  $\omega_h$ , the dimensionless cold dark matter energy density  $\omega_{\rm cdm}$ , the Hubble parameter today  $H_0$ , the logarithm of the variance of curvature perturbations centered around the pivot scale  $k_p = 0.05 \; \mathrm{Mpc^{-1}}$  (according to the Planck convention),  $\ln(10^{10}\mathcal{A}_s)$ , the scalar spectral index  $n_s$ , and the reionization optical depth  $\tau_{\rm reio}$ . Regarding the three free parameters of the EDE model, we impose a logarithmic prior on  $z_c$  and flat priors for  $f_{\text{EDE}}(z_c)$  and  $\Theta_i$ ,

$$3 \le \log_{10}(z_c) \le 4,$$
  
 $0 \le f_{\text{EDE}}(z_c) \le 0.5,$   
 $0 \le \Theta_i \le \pi.$ 

We define our MCMC chains to be converged when the Gelman-Rubin criterion R-1 < 0.05, except for runs combining Planck + EFTBOSS + ACT, for which we use a relaxed criterion of R-1 < 0.1 due to the complicated nature of the parameter space for the MCMC to explore. Finally, we extract the best-fit parameters from the procedure highlighted in the appendix of Ref. [48], and we produce our figures thanks to GetDist [146].

### C. Details on the BOSS measurements and EFT likelihoods

In this paper, we perform a thorough comparison of the constraints derived from the EFTBOSS data, in order to assess the consistency of the various analyses presented in the literature. Indeed, there are various BOSS two-point function measurements available to perform full-shape analyses, as well as a different EFT code. As described in more detail in Ref. [108], the BOSS DR12 data can be divided into two different sets of redshift splitting (LOWZ/ CMASS vs  $z_1/z_3$ ). Furthermore, depending on the estimator, the data are sometimes analyzed by convolving the theory model with a window function, or not. For a window-free analysis, one way is to use the configuration-space correlation function  $\xi$ , another is to use a quadratic estimator, which we denote with the subscript "QUAD." Finally, there are different ways to analyze the post-reconstructed parameters, which are then combined with the EFTBOSS data, denoted by  $\alpha_{\rm rec}$  and  $\beta_{\rm rec}$ . These different datasets include slightly different amounts of information (due to different scale cuts) but they all represent reasonable choices on how to analyze the BOSS DR12 observations.

The characteristics of each measurement are listed in Table I and more details can be found in Sec. IV of Ref. [108]. The EFT implementation and BOSS data we will focus on in this study are packaged in the PyBird likelihood, based on the EFT prediction and likelihood from PyBird<sup>15</sup> [101], and the CLASS-PT likelihood, based on the EFT prediction from CLASS-PT<sup>16</sup> [154] and likelihood from Ref. [39]. 17 Details about the PyBird and CLASS-PT likelihoods are presented in Sec. II of Ref. [108]. Here, let us simply mention that CLASS-PT implements the IRresummation scheme proposed in Ref. [155] and generalized to redshift space in Ref. [156]. This is different than that implemented in PyBird, proposed in Ref. [94], generalized to redshift space in Ref. [157], and made numerically efficient in Ref. [101]. The CLASS-PT scheme has been shown to be an approximation of the one used in PyBird in Ref. [158], where one considers only the resummation of the bulk displacements around the BAO peak,  $r_{\rm BAO} \sim$ 110 Mpc/h. For this scheme to be made practical, one further relies on a wiggle-no-wiggle split procedure to isolate the BAO part. Although this scheme has been shown to work fairly well within ACDM for cosmologies not too far from the one of Planck, we cautiously observe that in far-away cosmologies as the ones probed in EDE, the BAO peak location happens to be dramatically modified, and it thus remains to be checked that the approximations still hold in these cases. For our prior choice (on  $f_{\rm EDE}$ ), we have checked that at least the wiggle-no-wiggle split procedure as implemented in CLASS-PT is as numerically stable as for a fiducial case where the BAO peak is  $\sim 110 \text{ Mpc/}h$ .

In addition, in Ref. [108], we have checked the validity of the two pipelines by implementing in the PyBird likelihood the exact same prior as those used in the CLASS-PT likelihood, and we found agreement on the 1D posteriors of the cosmological parameters at  $\lesssim 0.2\sigma$  in  $\Lambda$ CDM, where these residual differences can be attributed to the different implementations of the IR-resummation mentioned above.

#### III. UPDATED EFTBOSS CONSTRAINTS ON EDE

#### A. Preliminary study

In the recent literature, there has been a number of analyses showing hints of EDE and allowing for a resolution of the Hubble tension [61,63,112–115]. In this preliminary study, we will take the results of two representative analyses. First, the baseline analysis of BaseTTTEEE + Lens + SH0ES data (second column of

<sup>&</sup>lt;sup>14</sup>Most parameters are converged at 0.01–0.05, the parameter with the worse convergence is  $\theta_i$ , which is often unconstrained or multimodal in the analyses.

<sup>15</sup>https://github.com/pierrexyz/pybird.

<sup>16</sup>https://github.com/michalychforever/CLASS-PT.

<sup>17</sup>https://github.com/oliverphilcox/full\_shape\_likelihoods.

TABLE II.  $\chi^2$  of each sky cut of the EFTBOSS dataset for the EDE best-fit models extracted from a fit to BaseTTTEEE + Lens + SH0ES and BaseTT650TEEE + ACT and the  $\Lambda$ CDM model from a fit to BaseTTTEEE + Lens + EFTBOSS. We also indicated the  $\Delta\chi^2$  with respect to the  $\Lambda$ CDM best-fit model. The associated p value is calculated assuming that the data points are uncorrelated and taking  $3 \cdot 9$  EFT parameters in each fit (given that the cosmology is fixed).

	$\begin{array}{c} BaseTTTEEE + Lens + \\ SH0ES  (EDE) \end{array}$	BaseTT650TEEE + ACT (EDE)	BaseTTTEEE + Lens + EFTBOSS (ΛCDM)
$\chi^2_{\text{CMASS NGC}}$	39.3	39.1	40.3
$\chi^2_{\text{CMASS SGC}}$	45.2	46.0	44.0
$\chi^2_{\text{LOWZ NGC}}$	34.4	35.1	33.5
$\chi^2_{\rm EFTBOSS}$	118.9	120.2	117.8
$\Delta \chi^2_{\min}(\text{EDE} - \Lambda \text{CDM})$	+1.1	+2.4	•••
p value (%)	16.7	14.7	18.5
$N_{\rm data}$		132	

Table III) has a best fit of  $f_{\rm EDE}(z_c) = 0.122$ ,  $H_0 = 71.89~{\rm km\cdot s^{-1}\cdot Mpc^{-1}}$ . Second, the analysis of BaseTT650TEEE + ACT (first column of Table IV) favors an EDE model with significantly larger values of  $f_{\rm EDE}(z_c)$  and  $H_0$  compared to the BaseTTTEEE + Lens + SH0ES, namely,  $f_{\rm EDE}(z_c) = 0.159$ ,  $H_0 = 73.30~{\rm km\cdot s^{-1}\cdot Mpc^{-1}}$  (see also [112–115]). In this section, we will gauge how these two specific models fair against BOSS data following Refs. [118,119].

Using the best-fit parameters listed in Table III (second column) and Table IV (first column), we perform a preliminary study where we determine the  $\chi^2$  of the EFTBOSS data (using our fiducial  $P_{\rm FKP}^{\rm LZ/CM} + \alpha_{\rm rec}^{\rm LZ/CM}$  data) after optimizing only the EFT parameters (since the cosmological parameters are fixed here). Using the PyBird code, we show in Table II the  $\chi^2$  associated with the EFTBOSS data, and we plot in Fig. 1 the residuals with respect to  $\Lambda$ CDM from the BaseTTTEEE + Lens + EFTBOSS

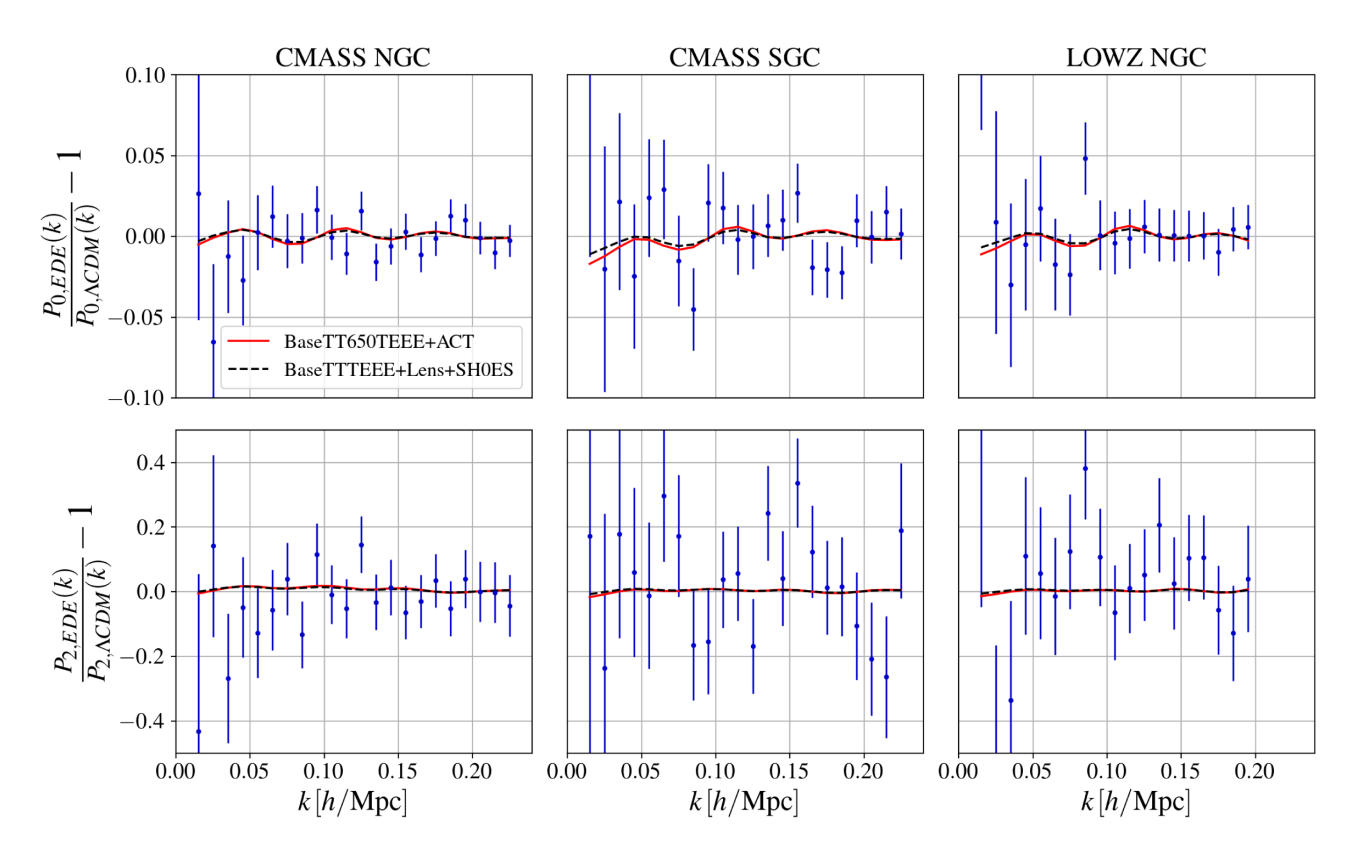


FIG. 1. Residuals of the monopole and quadrupole of the galaxy power spectrum in two EDE models (see Table II) with respect to the  $\Lambda$ CDM model (obtained from the baseTTTEEE + Lens + EFTBOSS analysis [103]) for the three sky cuts of the EFTBOSS data.

analysis <sup>18</sup> [103]. We also show the BOSS data residuals for comparison with respect to the same model. First, one can see that the changes in the residuals between those various fits are almost imperceptible by eye with respect to BOSS error bars. We find that the  $\chi^2$  of the BOSS data is degraded by +1.1 for BaseTTTEEE + Lens + SH0ES (to be compared with  $\sim +2.5$  in Ref. [118]) and +2.4 for BaseTT650TEEE + ACT, compared to the best fit  $\chi^2$  of EFTBOSS data in the  $\Lambda$ CDM model. Despite this small  $\chi^2$ degradation, we note that the p value of BOSS data in the EDE models that resolve the Hubble tension is still very good. Nevertheless, we anticipate that the EFTBOSS data could have a non-negligible constraining power in combination with BaseTT650TEEE + ACT, while its impact should be small in the context of the BaseTTTEEE + Lens + SH0ES analysis.

#### B. Constraints from various BOSS data

As is done in Ref. [108] for  $\Lambda$ CDM, we compare the constraints on EDE from the various BOSS two-point function measurements, described in Table I, in combination with the BBN prior on  $\omega_b$ .

The comparison of the 2D posteriors is shown in Fig. 2, while the 1D posteriors of  $\{f_{\rm EDE}(z_c), h, \omega_{\rm cdm}, \ln(10^{10}A_s), n_s, \Omega_m\sigma_8, S_8\}$  are shown in Fig. 3. In these figures, we also display the results from the BOSS data analyzed with the EFT predictions convolved with inconsistently normalized window functions, namely,  $\mathcal{P}_{\rm FKP}^{\rm LZ/CM} + \alpha_{\rm rec}^{\rm LZ/CM}$ , which disfavor the EDE model when they are combined with Planck data [118,119] (see the discussion in Appendix A for the impact of inconsistent normalization within the  $\Lambda$ CDM model). Interestingly, using the PyBird likelihood, the  $\Lambda$ CDM parameters are broadly consistent between  $P_{\rm FKP}^{\rm LZ/CM} + \alpha_{\rm rec}^{\rm LZ/CM}$  and  $P_{\rm QUAD}^{z_1/z_3} + \alpha_{\rm rec}^{z_1/z_3}$ , as we have a shift of  $\lesssim 0.3\sigma$  on  $\Lambda$ CDM parameters between these two measurements. However, we find that  $P_{\rm FKP}^{\rm LZ/CM} + \alpha_{\rm rec}^{\rm LZ/CM}$  leads to stronger constraints on EDE, namely,  $P_{\rm EDE}(z_c) < 0.321$ , while  $P_{\rm QUAD}^{z_1/z_3} + \alpha_{\rm rec}^{z_1/z_3}$  yields  $P_{\rm EDE}(z_c) < 0.382$ . Concerning  $\mathcal{E}^{\rm LZ/CM} + \alpha_{\rm rec}^{\rm LZ/CM}$ , we find different con-

Concerning  $\xi^{\text{LZ/CM}} + \alpha_{\text{rec}}^{\text{LZ/CM}}$ , we find different constraints, even for the  $\Lambda\text{CDM}$  parameters: comparing  $\xi^{\text{LZ/CM}} + \alpha_{\text{rec}}^{\text{LZ/CM}}$  to  $P_{\text{FKP}}^{\text{LZ/CM}} + \alpha_{\text{rec}}^{\text{LZ/CM}}$ , we find shifts of  $\lesssim 1.2\sigma$ , whereas comparing  $\xi^{\text{LZ/CM}} + \alpha_{\text{rec}}^{\text{LZ/CM}}$  to  $P_{\text{QUAD}}^{z_1/z_3} + \alpha_{\text{rec}}^{z_1/z_3}$ , we find shifts of  $\lesssim 1.0\sigma$ . Let us note that the constraints on  $\Lambda\text{CDM}$  parameters reconstructed from  $\xi^{\text{LZ/CM}} + \alpha_{\text{rec}}^{\text{LZ/CM}}$  are weaker than those of  $P_{\text{FKP}}^{\text{LZ/CM}} + \alpha_{\text{rec}}^{\text{LZ/CM}}$  and  $P_{\text{QUAD}}^{z_1/z_3} + \alpha_{\text{rec}}^{z_1/z_3}$ , which is consistent with what was found within the  $\Lambda\text{CDM}$  model in our companion paper [108] (see also

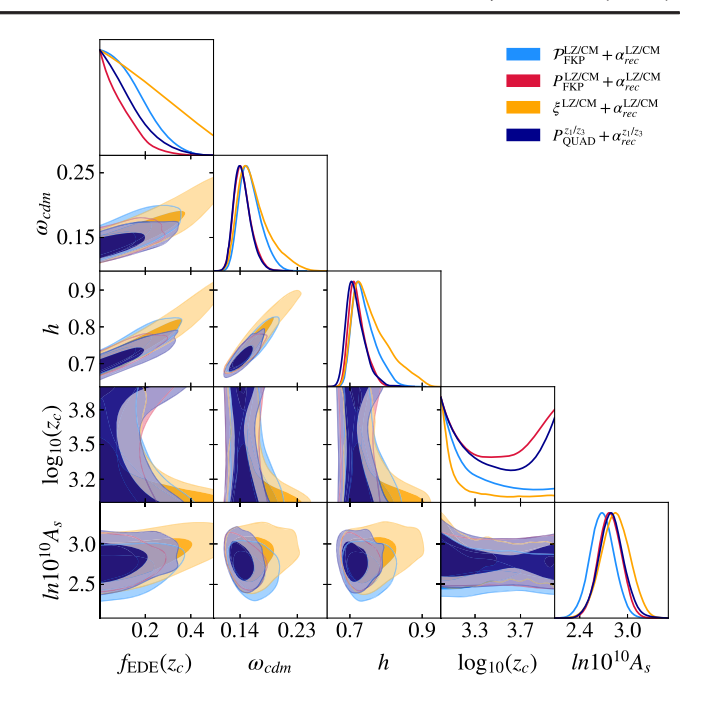


FIG. 2. Comparison of 2D posteriors of a subset of parameters in the EDE model reconstructed from BOSS full-shape analyses using PyBird baseline likelihood, with a BBN prior on  $\omega_b$ , of various pre-reconstructed two-point function measurements and handling of the window functions ( $\mathcal{P}_{FKP}^{LZ/CM}$ ,  $\mathcal{P}_{FKP}^{LZ/CM}$ ,  $\mathcal{E}_{FKP}^{LZ/CM}$ , which corresponds to  $\mathcal{E}_{FKP}^{LZ/CM}$ ,  $\mathcal{E}_{FKP}^{LZ/CM}$ ,  $\mathcal{E}_{FKP}^{LZ/CM}$ ,  $\mathcal{E}_{FKP}^{LZ/CM}$ . We choose to show only the cosmological parameters that are not completely prior dominated.

Ref. [38] and explanations therein). Regarding the EDE parameters, we obtain weaker constraints on  $f_{\rm EDE}$ , namely,  $f_{\rm EDE}(z_c) < 0.468$ . It is worth noting that, for the same likelihood, the constraints on  $f_{\rm EDE}(z_c)$  can be up to ~35% different depending on the data (especially between  $P_{\rm FKP}^{\rm LZ/CM} + \alpha_{\rm rec}^{\rm LZ/CM}$  and  $\xi^{\rm LZ/CM} + \alpha_{\rm rec}^{\rm LZ/CM}$ ). However, regardless of the data we consider, the BOSS full-shape (analyzed on their own with a BBN prior) within EDE leads to reconstructed values of  $H_0$  that are compatible with what is obtained by the SH0ES Collaboration.

This conclusion also holds for the CLASS-PT baseline (last line of Fig. 3), which is less constraining than the PyBird likelihood for the EDE model. Indeed, we obtain  $f_{\rm EDE}(z_c) < 0.448$ , which is ~15% weaker than the constraint obtained with the PyBird likelihood, even for similar data ( $P_{\rm QUAD}^{z_1/z_3}$ ). Furthermore, we note that the  $f_{\rm EDE}(z_c)$  constraint reconstructed from  $P_{\rm FKP}^{\rm LZ/CM} + \alpha_{\rm rec}^{\rm LZ/CM}$ , analyzed with the PyBird likelihood, is ~35% weaker than the constraint obtained from  $P_{\rm QUAD}^{z_1/z_3} + \beta_{\rm rec}^{z_1/z_3}$ , analyzed with

<sup>&</sup>lt;sup>18</sup>When combined with EFTBOSS, we do not include the BOSS BAO  $+ f\sigma_8$  data.

<sup>&</sup>lt;sup>19</sup>Per convention, we cite one-sided bound at 95% C.L. and two-sided ones at 68% C.L.

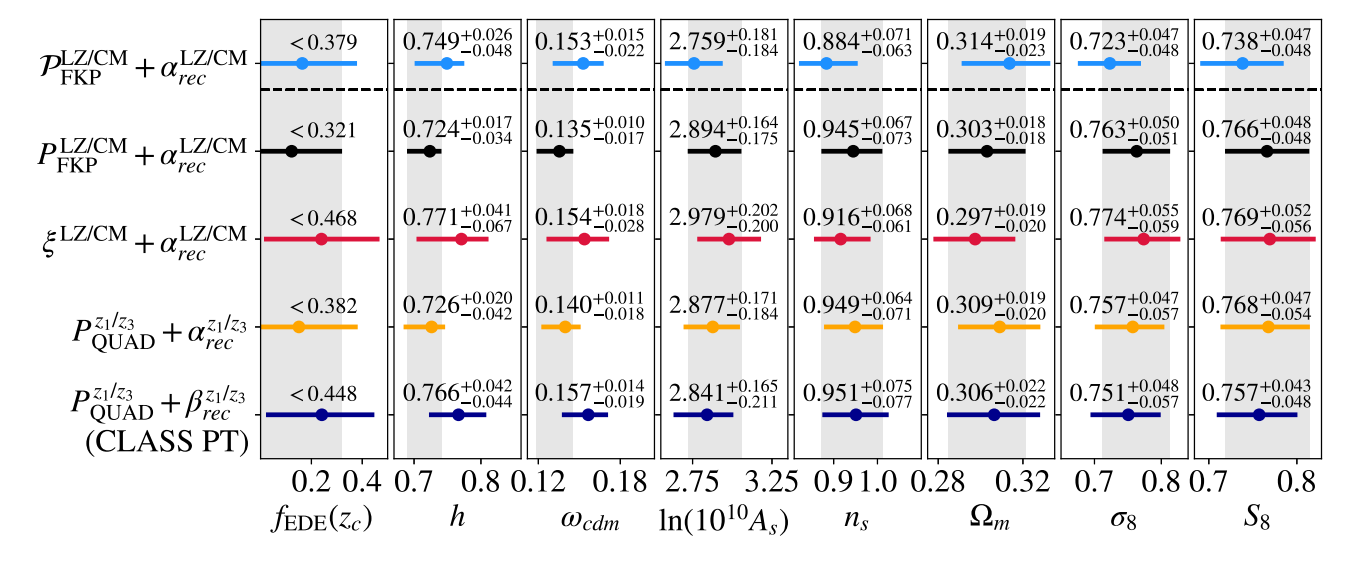


FIG. 3. Comparison of 1D credible intervals in the EDE model reconstructed from BOSS full-shape analyses using PyBird baseline likelihood, with a BBN prior on  $\omega_b$ , of various pre-reconstructed two-point function measurements and handling of the window functions  $(\mathcal{P}_{\text{FKP}}^{\text{LZ/CM}}, P_{\text{FKP}}^{\text{LZ/CM}}, \xi^{\text{LZ/CM}}, P_{\text{QUAD}}^{z_1/z_3})$  combined with various post-reconstructed BAO parameters  $(\alpha_{\text{rec}}^{\text{LZ/CM}}, \alpha_{\text{rec}}^{z_1/z_3}, \alpha_{\text{rec}}^{z_1/z_3})$ . We recall that  $\mathcal{P}_{\text{FKP}}^{\text{LZ/CM}} + \alpha_{\text{rec}}^{\text{LZ/CM}}$  corresponds to the BOSS FKP measurements analyzed with the EFT predictions convolved with inconsistently normalized window functions. The gray region corresponds to the EFTBOSS data that we use in our main analysis, namely,  $P_{\text{FKP}}^{\text{LZ/CM}} + \alpha_{\text{rec}}^{\text{LZ/CM}}$ . In the last line, we also show the results of  $P_{\text{QUAD}}^{z_1/z_3} + \beta_{\text{rec}}^{z_1/z_3}$  analyzed using the CLASS-PT baseline likelihood. Relevant information regarding the measurements and their notations are summarized in Table I. We choose to show only the cosmological parameters that are not prior dominated. For  $f_{\text{EDE}}$ , we quote instead the  $2\sigma$  bound.

the CLASS-PT likelihood. We conclude that the standard PyBird analysis setup (which consists of our baseline setup) shows a higher constraining power than the standard CLASS-PT analysis. Let us note that, for the  $H_0$  parameter, we obtain a value  $1.4\sigma$  higher than the Planck value  $(h = 0.6851^{+0.0076}_{-0.014} \text{ at } 68\% \text{ C.L.})$  with the PyBird analysis setup and a value  $1.8\sigma$  higher with the CLASS-PT analysis setup, which indicates a reasonably good consistency between Planck and BOSS regarding  $H_0$ . For a more detailed discussion, including other data combinations, of the differences between PyBird and CLASS-PT for the EDE model, we refer to Appendix B. We, however, warn that the cosmological constraints from EFTBOSS at the level of the 1D posteriors might be affected by prior effects, as discussed in our companion paper [108] in the context of  $\Lambda$ CDM.

#### C. Primary CMB-free constraints on EDE

To fully gauge the constraining power of a primary CMB-free analysis, on top of the fiducial EFTBOSS data and BBN prior, we now include other BOSS BAO measurements, Planck lensing, and the Pantheon18 datasets. We recall that this dataset is simply called BaseEFTBOSS, and we plot the associated reconstructed 2D posteriors in Fig. 4 (blue contours). We compare our results with the posteriors reconstructed from a BaseTTTEEE + Lens + SH0ES (red contours) and BaseTT650TEEE + ACT (orange contours) analysis. One can see that, while the primary CMB-free

analysis does not favor EDE (in the absence of a SH0ES prior), constraints are relatively weak and the reconstructed posteriors from the BaseEFTBOSS data are not in tension with those reconstructed from the BaseTTTEEE + Lens + SH0ES and BaseTT650TEEE + ACT analyses. Nevertheless, we note a clear narrowing of the constraints in the  $\{f_{\rm EDE}(z_c), \log_{10}(z_c)\}$  parameter space around  $\log_{10}(z_c) \sim 3.5$ , indicating that BOSS gains constraining power right around matter-radiation equality. To extract a meaningful CMB-independent bound on  $f_{\rm EDE}(z_c)$ , we perform an additional analysis now restricting the  $\log_{10}(z_c)$  range to  $\log_{10}(z_c) \in [3.4, 3.7]$ , which corresponds to the region favored to resolve the Hubble tension. We find that the combination of EFTBOSS + BBN + Lens + BAO + Pan18 (i.e., BaseEFTBOSS) leads to  $f_{\rm EDE}(z_c) < 0.2$  (95% C.L.) and  $h = 0.710^{+0.015}_{-0.025}$ , which does not exclude the EDE models resolving the Hubble tension. When performing the same analysis with CLASS-PT, we find significantly weaker constraints, with  $f_{\rm EDE}(z_c)$  < 0.284 (95% C.L.) and  $h = 0.726^{+0.02}_{-0.04}$ . Constraints from CLASS-PT are shown in Appendix B, Fig. 9.

# IV. EFTBOSS COMBINED WITH CMB DATA A. EFTBOSS + PlanckTTTEEE

We now turn to studying the constraining power of EFTBOSS data in combination with primary CMB datasets. We start by performing joint analyses with the full

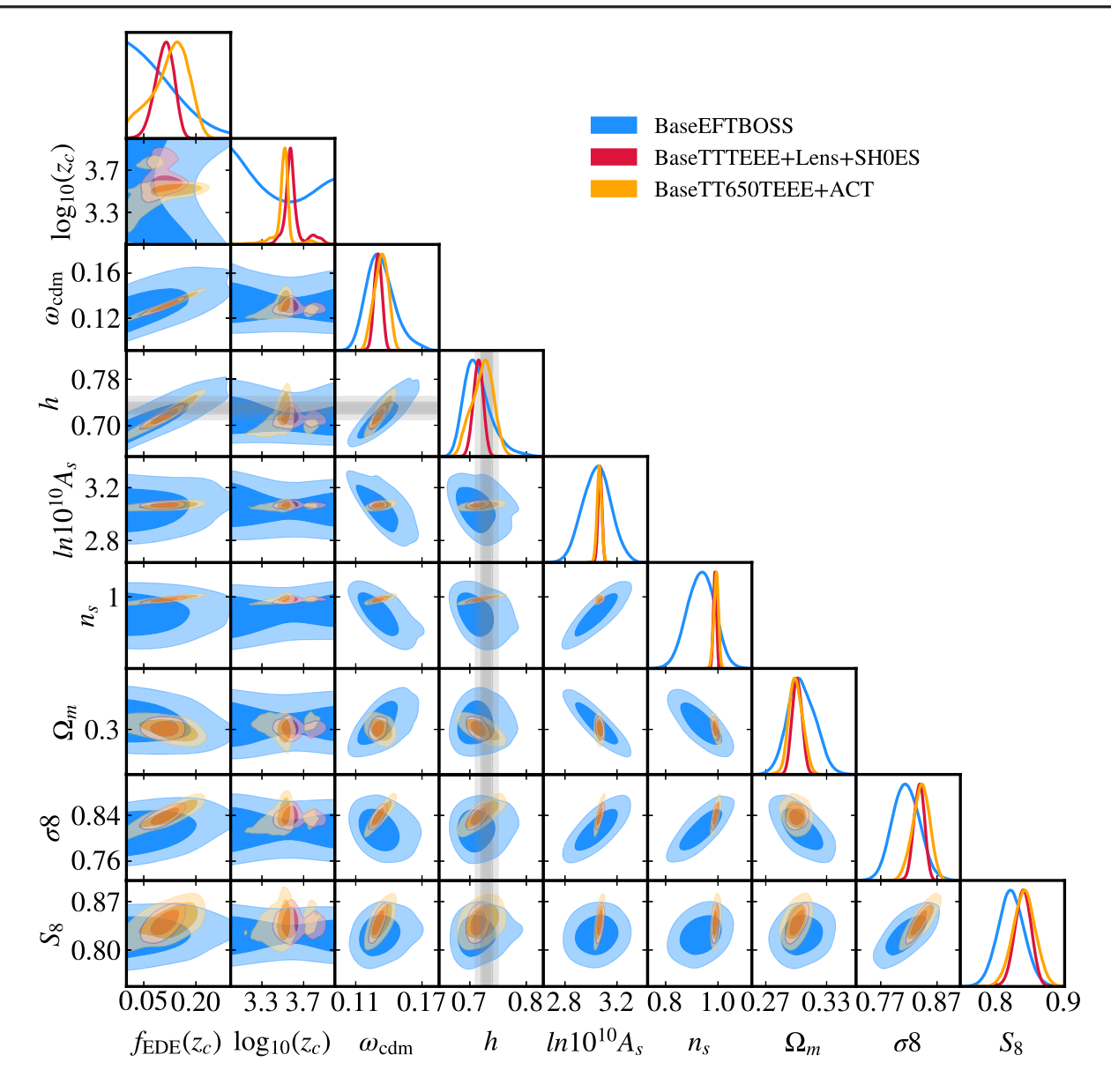


FIG. 4. 2D posterior distributions reconstructed from the BaseEFTBOSS dataset compared with the posterior reconstructed from BaseTTTEEE + Lens + SH0ES and BaseTT650TEEE + ACT. We recall that BaseEFTBOSS refers to EFTBOSS + BBN + Lens + BAO + Pan18, BaseTTTTEEE refers to Planck TTTEE + BAO + Pan18, and BaseTT650TEEE to Planck TT650TEE + BAO + Pan18.

PlanckTTTEEE datasets. All relevant  $\chi^2$  statistics are given in Appendix C, Tables VII and VIII, while the reconstructed posteriors and best-fit values of parameters are given in Table III. In the left panel of Fig. 5, we compare constraints obtained with the consistently and inconsistently normalized EFTBOSS data to that obtained with the compressed BAO/ $f\sigma_8$  data. One can see that the correction of the normalization of the window function leads the new EFTBOSS data to have a constraining power only slightly stronger than the compressed BAO/ $f\sigma_8$  data. We derive a BaseTTTEEE + Lens + EFTBOSS constraint of  $f_{\rm EDE}(z_c) < 0.083$ , to be compared with  $f_{\rm EDE}(z_c) < 0.088$  from BaseTTTEEE + Lens +  $f\sigma_8$ , while the

EFTBOSS data with wrong normalization incorrectly lead to  $f_{\rm EDE}(z_c) < 0.054$ .

Moreover, as was already pointed out in various works [48,120,121,123], posteriors are highly non-Gaussian with long tails toward high  $H_0$ , and therefore these constraints should be interpreted with care. This is further attested by the fact that the best-fit point lies at the  $2\sigma$  limit of our constraints (e.g.,  $f_{\rm EDE}$  at the best fit is 0.082 for BaseTTTEEE + Lens + EFTBOSS). We defer to future work to compare constraints derived here with a Bayesian analysis to those derived with a profile likelihood approach (e.g., [123,124]), which will be affected by our update to the survey window function calculation.

TABLE III. Mean (best fit)  $\pm 1\sigma$  (or  $2\sigma$  for one-sided bounds) of reconstructed parameters in the EDE model confronted to various datasets, including Planck TTTEEE.

	BaseTTTEEE+Lens		BaseTTTEEE	$1 + \text{Lens} + f\sigma_8$	BaseTTTEEE + Lens + EFTBOSS		
$H_0$ prior?	No	Yes	No	Yes	No	Yes	
$f_{\text{EDE}}(z_c)$	< 0.091 (0.088)	$0.109(0.122)^{+0.030}_{-0.024}$	< 0.088(0.057)	$0.102(0.118)^{+0.030}_{-0.024}$	< 0.083(0.082)	$0.103(0.116)^{+0.027}_{-0.023}$	
$\log_{10}(z_c)$	Unconstrained (3.55)	$3.599(3.568)^{+0.029}_{-0.081}$	Unconstrained (3.78)	$3.603(3.569)^{+0.037}_{-0.11}$	Unconstrained (3.82)	$3.67(3.83)^{+0.21}_{-0.15}$	
$\theta_i$	Unconstrained (2.8)	$2.65(2.73)^{+0.22}_{-0.025}$	Unconstrained (2.94)	$2.58(2.76)_{+0.034}^{+0.33}$	Unconstrained (2.9)	$2.73(2.89)^{+0.19}_{-0.065}$	
h	$0.688(0.706)^{+0.006}_{-0.011}$	$0.715(0.719) \pm 0.009$	$0.687(0.694)^{+0.006}_{-0.011}$	$0.712(0.718) \pm 0.009$	$0.687(0.700)^{+0.006}_{-0.011}$	$0.713(0.715)\pm0.009$	
$\omega_{ m cdm}$	$0.1227(0.1281)^{+0.0018}_{-0.0036}$	$0.1303 (0.1319) \pm 0.0035$	$0.1227(0.1246)^{+0.0016}_{-0.0036}$	$0.1296 (0.1314) \pm 0.0035$	$0.1221(0.1269)^{+0.0015}_{-0.0033}$	$0.1288 (0.1297) \pm 0.0032$	
$10^2 \omega_b$	$2.258(2.266)^{+0.018}_{-0.020}$	$2.283(2.303) \pm 0.020$	$2.258(2.266)^{+0.017}_{-0.021}$	$2.282(2.279) \pm 0.021$	$2.257(2.275)^{+0.017}_{-0.020}$	$2.287(2.301) \pm 0.023$	
$10^{9}A_{s}$	$2.122(2.135) \pm 0.032$	$2.153(2.145) \pm 0.032$	$2.119(2.119)^{+0.029}_{-0.033}$	$2.146(2.164)\pm0.031$	$2.113(2.120) \pm 0.032$	$2.144(2.144) \pm 0.032$	
$n_s$	$0.9734(0.9823)^{+0.0053}_{-0.0076}$	$0.9883 (0.9895) \pm 0.0060$	$0.9730(0.9809)^{+0.0048}_{-0.0074}$	$0.9868 (0.9899) \pm 0.0062$	$0.9715(0.9827)^{+0.0049}_{-0.0076}$	$0.9867 (0.9921) \pm 0.0065$	
$ au_{ m reio}$	$0.0570(0.0574)^{+0.0069}_{-0.0076}$	$0.0582 (0.0579) \!\pm\! 0.0075$	$0.0564(0.0553) \pm 0.0072$	$0.0572(0.059) \pm 0.0073$	$0.0562(0.0553)\pm0.0073$	$0.0586(0.0599)^{+0.0068}_{-0.0076}$	
$S_8$	$0.831(0.839)^{+0.011}_{-0.013}$	$0.839 (0.843) \pm 0.012$	$0.831(0.833)^{+0.011}_{-0.012}$	$0.838 (0.843) \pm 0.013$	$0.826(0.836)\pm0.011$	$0.833(0.835) \pm 0.012$	
$\Omega_m$		$0.3008 (0.3005) \!\pm\! 0.0048$	$0.3089(0.3074)\pm0.0054$	$0.3019 (0.3003) \pm 0.0051$	$0.3077 (0.3065) \pm 0.0054$	$0.2998 (0.3004) \pm 0.0050$	
Total $\chi^2_{\min}$	3799.2	3802.9	3801.8	3806.1	3912.7	3917.3	
$\Delta\chi^2_{\rm min}$	-3.8	-23.7	-3.9	-23.0	-4.7	-22.7	
$Q_{\mathrm{DMAP}}$	1.	$9\sigma$	2.	$2.0\sigma$		$2.1\sigma$	

As advocated recently, we will gauge the level of the Hubble tension by computing the tension metric  $Q_{\rm DMAP} \equiv \sqrt{\chi^2({\rm w/SH0ES}) - \chi^2({\rm w/oSH0ES})}$  [48,159], which agrees with the usual Gaussian metric tension for Gaussian posteriors, but better captures the non-Gaussianity of the posterior.

Once the SH0ES prior is included in the BaseTTTEEE + Lens + EFTBOSS analysis, we reconstruct  $f_{\rm EDE}(z_c) = 0.103^{+0.027}_{-0.023}$  with  $h = 0.713 \pm 0.009$  and find the tension metric  $Q_{\rm DMAP} = 2.1\sigma$  (while we find 4.8 $\sigma$  in  $\Lambda$ CDM), see Table III and Fig. 5, right panel. This is only a minor difference compared to the results without BOSS  $f\sigma_8$  or

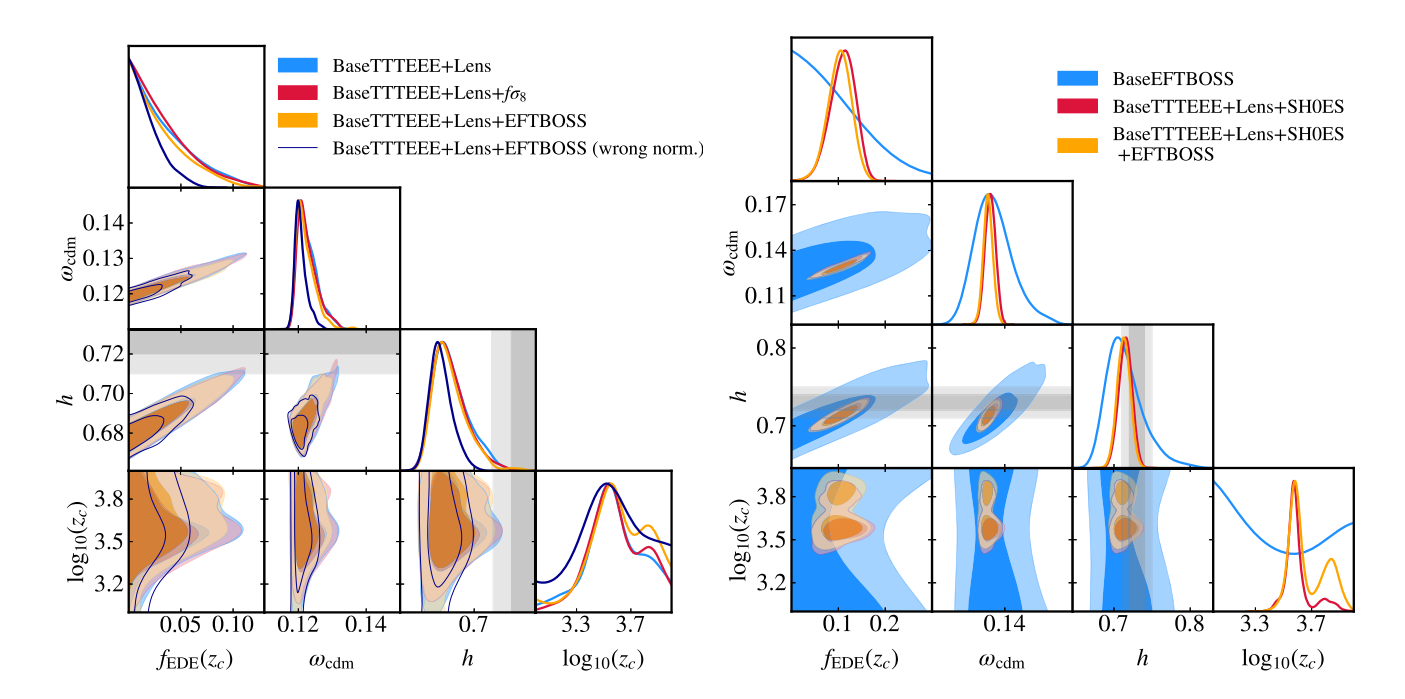


FIG. 5. Left: 2D posterior distributions from BaseTTTEEE+Lens, BaseTTTEEE+Lens+ $f\sigma_8$ , and BaseTTTEEE+Lens+EFTBOSS. We also show the results from the EFTBOSS data with a wrong normalization for comparison. Right: 2D posterior distributions from BaseEFTBOSS and BaseTTTTEEE+Lens+SH0ES, with and without EFTBOSS data. We recall that BaseTTTTEEE refers to Planck TTTEE+BAO+Pan18, while BaseEFTBOSS refers to EFTBOSS+BBN+Lens+BAO+Pan18.

TABLE IV. Mean (best fit)  $\pm 1\sigma$  (or  $2\sigma$  for one-sided bounds) of reconstructed parameters in the EDE model confronted to various datasets, including Planck TT650TEEE + ACT.

	BaseTT650TEEE + ACT	$\begin{array}{c} \text{BaseTT650TEEE} + \\ \text{ACT} + f\sigma_8 \end{array}$	BaseTT650TEEE + ACT + EFTBOSS	$\begin{array}{c} BaseTT650TEEE + ACT + \\ Lens + EFTBOSS \end{array}$
$f_{\text{EDE}}(z_c)$	$0.128(0.159)^{+0.064}_{-0.039}$	$0.116(0.148)^{+0.059}_{-0.046}$	$0.093(0.148)^{+0.047}_{-0.066}$	<0.172(0.148)
$\log_{10}(z_c)$	$3.509(3.521)^{+0.048}_{-0.033}$	$3.505(3.514)_{-0.049}^{+0.056}$	$3.493(3.514)^{+0.080}_{-0.093}$	$3.486(3.514)_{-0.13}^{+0.091}$
$ heta_i$	$2.63(2.77)^{+0.24}_{+0.023}$	$2.53(2.78)_{+0.094}^{+0.37}$	$2.54(2.78)_{0.065}^{+0.47}$	$2.41(2.78)_{0.12}^{+0.65}$
h	$0.723(0.733)^{+0.021}_{-0.017}$	$0.718(0.728) \pm 0.018$	$0.713(0.730)^{+0.017}_{-0.021}$	$0.708(0.725)^{+0.015}_{-0.022}$
$\omega_{ m cdm}$	$0.1332(0.1369)^{+0.0071}_{-0.0059}$	$0.1320(0.1355) \pm 0.0062$	$0.1285(0.1355)^{+0.021}_{-0.0067}$	$0.1276(0.1355)^{+0.0047}_{-0.0074}$
$10^2 \omega_h$	$2.268(2.267) \pm 0.019$	$2.266(2.261) \pm 0.020$	$2.265(2.266) \pm 0.020$	$2.263(2.265) \pm 0.019$
$10^{9}A_{s}$	$2.144(2.148) \pm 0.037$	$2.136(2.144) \pm 0.038$	$2.128(2.147) \pm 0.040$	$2.127(2.143) \pm 0.034$
$n_s$	$0.9928(0.9963)^{+0.0092}_{-0.0078}$	$0.9910(0.9936)^{+0.0090}_{-0.0081}$	$0.9885(0.9936) \pm 0.0091$	$0.9865(0.9936) \pm 0.0086$
$ au_{ m reio}$	$0.0520(0.0508) \pm 0.0077$	$0.0511(0.0506) \pm 0.0079$	$0.0519 (0.0506) \pm 0.0077$	$0.0523(0.0506) \pm 0.0072$
$S_8$	$0.842(0.846) \pm 0.016$	$0.841(0.845) \pm 0.017$	$0.830(0.838) \pm 0.016$	$0.831(0.837)_{-0.014}^{+0.013}$
$\Omega_m$	$0.2996(0.2982)^{+0.0061}_{-0.0072}$	$0.3013(0.2995) \pm 0.0068$	$0.2990(0.2995) \pm 0.0069$	$0.3008(0.2995) \pm 0.0059$
Total $\chi^2_{\rm min}$	3571.9	3575.8	3688.3	3698.4
$\Delta \chi^2 (\text{EDE} - \Lambda \text{CDM})$	-14.6	-13.3	-12.0	-11.1

full-shape information, for which we get  $f_{\rm EDE}(z_c) = 0.109^{+0.030}_{-0.024}$  with  $h = 0.715 \pm 0.009$  and the  $Q_{\rm DMAP}$  metric gives a  $1.9\sigma$  tension between SH0ES and other datasets. Similarly, when the  $f\sigma_8$  information is included, we find a  $2.0\sigma$  tension with  $f_{\rm EDE}(z_c) = 0.102^{+0.030}_{-0.024}$  and  $h = 0.712 \pm 0.009$ .

Analyses with CLASS-PT are presented in Appendix B, and similar results are found. Therefore, current full-shape EFTBOSS data provide little additional constraining power ( $\sim 10\%$ ) on the EDE model over Planck and  $f\sigma_8$ . We conclude that the EFTBOSS data are in agreement with the model reconstructed when including a SH0ES prior, as the preliminary study suggested, and BOSS data do not exclude the EDE resolution to the Hubble tension.

#### B. EFTBOSS + PlanckTT650TEE + ACT

We now turn to the combination of Planck data with ACT. We start with a restricted version of Planck temperature data at  $\ell < 650$  (chosen to mimic WMAP and perform a consistency test between CMB datasets), combined with Planck polarization and ACT data. This data combination<sup>21</sup> is known to favor<sup>22</sup> EDE at  $\sim 3\sigma$  [112–115], with large values of  $f_{\rm EDE}(z_c) = 0.128^{+0.064}_{-0.039}$  and  $h = 0.723^{+0.021}_{-0.017}$  (see Table IV, first column). In Ref. [115], it

was shown that BOSS  $f\sigma_8$  and Planck lensing data decreased the preference  $^{23}$  to  $2.6\sigma$ . We now test whether the EFT analysis of BOSS data can put further pressure on this hint of EDE, as our preliminary study indicates. All relevant  $\chi^2$  statistics are given in Appendix C, Table IX, while we give the reconstructed posteriors of parameters in Table IV. We show in Fig. 6 (left panel) the 2D posterior distribution  $\{f_{\rm EDE}(z_c), \omega_{\rm cdm}, h, \log_{10}(z_c)\}$  reconstructed from the analysis of BaseTT650TEEE + ACT compared with that reconstructed with the addition of either  $f\sigma_8$  or EFTBOSS data.

One can see that, in this case, the EFTBOSS data do reduce the preference for EDE, with  $f_{\rm EDE}$  now compatible with zero at  $1\sigma$ . For the BaseTT650TEEE + ACT + Lens + EFTBOSS dataset, represented by the dark blue line on Fig. 6 (left panel), we find a weak upper limit  $f_{\rm EDE} < 0.172$  and  $h = 0.708^{+0.015}_{-0.022}$ , with best-fit values  $f_{\rm EDE} \simeq 0.148$  and  $h \simeq 0.725$  in good agreement with the SH0ES determination. Quantifying the preference over  $\Lambda$ CDM, we find a  $\Delta \chi^2 = -11.1$  in favor of EDE (2.5 $\sigma$ ), decreased from -14.6 without EFTBOSS and Planck lensing data. The  $\chi^2$  of EFTBOSS data is degraded by +1.7 in the EDE model compared to  $\Lambda$ CDM, while the improvement in the fit of ACT and Planck TT650TEEE is fairly stable, with  $\Delta \chi^2(ACT) = -7.6$  $\Delta \chi^2$ (PlanckTT650TEEE) = -6.1, Additionally, we note that, for this more extreme EDE

<sup>&</sup>lt;sup>20</sup>This is different than what was reported in Ref. [48], because of an updated  $H_0$  prior with tighter error bars.

<sup>&</sup>lt;sup>21</sup>The preference persists until PlanckTT data at  $\ell \gtrsim 1300$  are included, while the inclusion of SPT-3G TEEE data has little impact (in fact, slightly strengthening the hint of EDE) [115].

<sup>&</sup>lt;sup>22</sup>As discussed by the ACT Collaboration [112], it is still a possibility that the apparent preference for EDE arises from remaining systematic errors in the data.

 $<sup>^{23}</sup>$ In the following, the preference is computed assuming the  $\Delta \chi^2$  follows a  $\chi^2$  distribution with 3 degrees of freedom. We stress that this is just an approximation, as the true number of degrees of freedom is more complicated to estimate due to  $\log_{10}(z_c)$  and  $\theta_i$  becoming ill defined when  $f_{\rm EDE} \rightarrow 0$ .

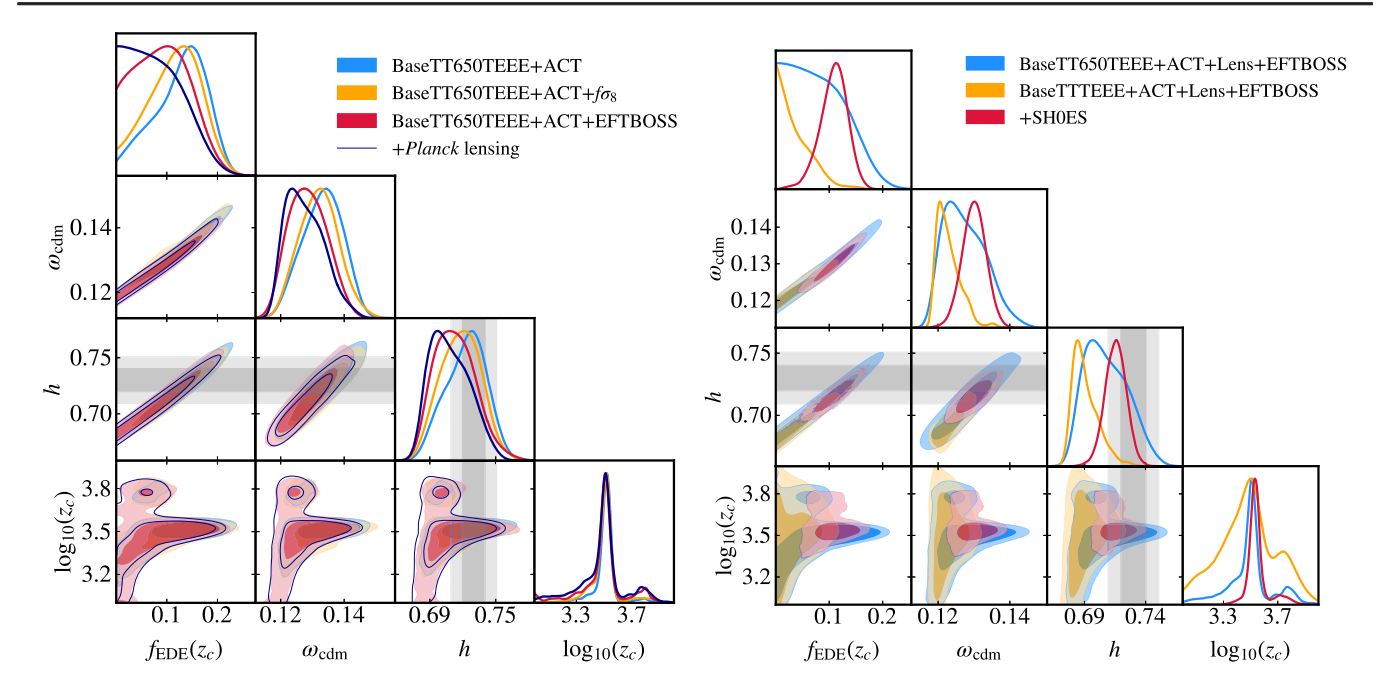


FIG. 6. Left: 2D posterior distributions from BaseTT650TEEE + ACT in combination with  $f\sigma_8$ , EFTBOSS, and Planck lensing. We recall that BaseTT650TEEE refers to Planck TT650TEEE + BAO + Pan18 data. Right: 2D posterior distributions from ACT + Lens + EFTBOSS in combination with either BaseTT650TEEE or BaseTTTEEEE with and without SH0ES.

model, the full EFTBOSS data provide stronger constraints than the conventional BAO/ $f\sigma_8$  data. Although current data do not fully erase the preference for EDE over  $\Lambda$ CDM, this confirms that BOSS data, and more generally measurement of the matter power spectrum in the late Universe, provide an important probe of large EDE fraction in the early Universe. We find similar results with CLASS-PT (see Appendix B for details), attesting that once BOSS data are

combined with CMB data, the results obtained are robust to reasonable choices in the EFT analysis.

#### C. EFTBOSS + PlanckTTTEE + ACT

Except for consistency tests, there are no good reasons to remove part of the high- $\ell$  Planck TT data. In the following, we present results of combined analyses of

TABLE V. Mean (best fit)  $\pm 1\sigma$  (or  $2\sigma$  for one-sided bounds) of reconstructed parameters in the EDE model confronted to BaseTTTEEE + ACT + Lens + EFTBOSS, with and without SH0ES.

	BaseTTTEEE + ACT + Lens + EFTBOSS				
$H_0$ prior?	No	Yes			
$f_{\rm EDE}(z_c)$	<0.110(0.074)	$0.108(0.124)^{+0.028}_{-0.021}$			
$\log_{10}(z_c)$	$3.48(3.51) \pm 0.21$	$3.552(3.531)_{-0.065}^{+0.026}$			
$ heta_i$	Unconstrained	$2.77(2.81)_{-0.070}^{+0.13}$			
h	$0.691(0.7)_{-0.013}^{+0.006}$	$0.715(0.72) \pm 0.009$			
$\omega_{ m cdm}$	$0.1229(0.1267)^{+0.0017}_{-0.0042}$	$0.1300(0.1322)^{+0.0035}_{-0.0031}$			
$10^2 \omega_b$	$2.247(2.248)^{+0.015}_{-0.017}$	$2.260(2.255) \pm 0.018$			
$10^{9}A_{s}$	$2.126(2.133)^{+0.028}_{-0.032}$	$2.153(2.156) \pm 0.030$			
$n_s$	$0.9758(0.9795)^{+0.0049}_{-0.0080}$	$0.9873(0.9893) \pm 0.0058$			
$ au_{ m reio}$	$0.0540(0.0534) \pm 0.0070$	$0.0548 (0.0539) \pm 0.0070$			
$S_8$	$0.829(0.843)^{+0.010}_{-0.012}$	$0.837(0.843) \pm 0.012$			
$\Omega_m$	$0.3061(0.3052) \pm 0.0054$	$0.2997(0.3) \pm 0.0047$			
Total $\chi^2_{\rm min}$	4157.6	4159.8			
$\Delta \chi^2_{\min}(\text{EDE} - \Lambda \text{CDM})$	-6.4	-26.1			
$Q_{ m DMAP}$	1.	$5\sigma$			

TABLE VI. Mean (best fit)  $\pm 1\sigma$  (or  $2\sigma$  for one-sided bounds) of reconstructed parameters in the EDE model confronted to various datasets, including the recent PanPlus SNIa catalog.

	BaseEFTBOSS + PanPlus	BaseTTTEEE + Lens + EFTBOSS + PanPlus	BaseTTTEEE + Lens + EFTBOSS + PanPlus + SH0ES	BaseTT650TEEE + ACT + Lens + EFTBOSS + PanPlus
$f_{\text{EDE}}(z_c)$	< 0.228(0.01)	< 0.079(0.056)	$0.123(0.141)^{+0.030}_{-0.018}$	< 0.137(0.11)
$\log_{10}(z_c)$	Unconstrained (3.91)	$3.59(3.57)_{-0.21}^{+0.25}$	$3.64(3.57)_{-0.13}^{+0.23}$	<3.5(3.5)
$ heta_i$	Unconstrained (2.98)	Unconstrained (2.74)	$2.59(2.77)_{+0.064}^{+0.31}$	Unconstrained (2.78)
h	$0.717(0.692)^{+0.015}_{-0.026}$	$0.684(0.692)_{-0.001}^{+0.006}$	$0.719(0.724)_{-0.008}^{+0.009}$	$0.700(0.714)^{+0.013}_{-0.019}$
$\omega_{ m cdm}$	$0.142(0.131)^{+0.010}_{-0.014}$	$0.1222(0.1251)^{+0.0015}_{-0.0028}$	$0.1317(0.1346) \pm 0.0031$	$0.1258(0.1306)^{+0.0039}_{-0.0058}$
$10^{-2}\omega_{b}$	$2.276(0.023)_{-0.039}^{+0.035}$	$2.251(2.254) \pm 0.018$	$2.291(2.275)^{+0.020}_{-0.024}$	$2.258(2.259) \pm 0.019$
$10^{9}A_{s}$	$1.88(1.929)_{-0.20}^{+0.16}$	$2.114(2.148) \pm 0.029$	$2.155(2.157)^{+0.030}_{-0.036}$	$2.120(2.135) \pm 0.033$
$n_s$	$0.873(0.889) \pm 0.049$	$0.9700(0.9752)^{+0.0046}_{-0.0071}$	$0.9911(0.9912)^{+0.0062}_{-0.0071}$	$0.9827(0.9877) \pm 0.0081$
$ au_{ m reio}$		$0.0562(0.0558) \pm 0.0069$	$0.0582(0.0554) \pm 0.0077$	$0.0519(0.0516)^{+0.0065}_{-0.0075}$
$S_8$	$0.815(0.824) \pm 0.018$	$0.832(0.837) \pm 0.010$	$0.840(0.847) \pm 0.012$	$0.831(0.839)^{+0.012}_{-0.011}$
$\Omega_m$	$0.321(0.324) \pm 0.013$	$0.3116(0.3093) \pm 0.0056$	$0.3000(0.3014) \pm 0.0047$	$0.3041(0.3016) \pm 0.0061$
Total $\chi^2_{\rm min}$	1537.9	4304.0	4187.0	4085.1
$\Delta \chi^2_{\min} (\text{EDE} - \Lambda \text{CDM})$	0	-1.1	-32.3	-9.2

PlanckTTTEEE + ACT + EFTBOSS (i.e., including full Planck data) in Table V and Fig. 6 (right panel). All relevant  $\chi^2$  statistics are given in Appendix C, Table X. We quantify the residual tension with SH0ES using the  $Q_{\text{DMAP}}$  metric introduced previously. In that case, we find that the preference for EDE without SH0ES is strongly reduced, in agreement with previous works, but the  $2\sigma$  upper limit on  $f_{\rm EDE} < 0.110$  is much weaker than in the BaseTTTEEE + previously, Lens + EFTBOSSanalysis presented  $f_{\rm EDE}$  < 0.083. As a result, the tension metric between BaseTTTEEE + ACT + Lens + EFTBOSS and SH0ES is released to  $1.5\sigma$  compared to  $4.7\sigma$  in  $\Lambda$ CDM (and  $2.1\sigma$ without ACT data). When the SH0ES prior is included, we find  $f_{\rm EDE} = 0.108^{+0.028}_{-0.021}$  and  $h = 0.715 \pm 0.009$  (in very good agreement with the results presented earlier without ACT), with no degradation in the  $\chi^2$  of EFTBOSS. This confirms that the EFTBOSS data can accommodate the amount of EDE required to resolve the Hubble tension (with  $f_{\rm EDE} \sim 0.1$  and  $h \sim 0.72$ ), but constrain more extreme EDE contributions.

#### D. Impact of Pantheon + data

To finish, we perform an analysis with the new Pantheon+ SNIa catalog [127], which is known to favor a higher  $\Omega_m = 0.338 \pm 0.018$ , to illustrate the impact that these new data have on the EDE model. We perform analyses of four datasets in combination with Pantheon+, following our baseline data, namely, BaseEFTBOSS, BaseTTTEEE + Lens + EFTBOSS(+SH0ES), and BaseTT650TEEE+ACT+Lens+EFTBOSS. The results of these analyses are presented in Table VI and in Fig. 7, while all relevant  $\chi^2$  statistics are given in

Appendix C, Table XI. First, without information from the primary CMB, we find that the combination EFTBOSS + BBN + Lens + BAO + PanPlusBaseEFTBOSS + PanPlus) leads to a weak constraint on  $f_{\rm EDE}(z_c) < 0.228$  with  $h = 0.717^{+0.015}_{-0.026}$  in good agreement with SH0ES. In fact, even within  $\Lambda {\rm CDM}$  we find  $h = 0.694^{+0.012}_{-0.014}$ , which is not in significant tension with SH0ES. This data combination was recently argued to constrain new physics solution to the Hubble tension that affects the sound horizon, due to the fact that measurement of h based on the scale of matter-radiation equality  $k_{eq}$ (which can be extracted by marginalizing over the sound horizon information<sup>24</sup>) is in tension with the SH0ES measurement [39,126,151]. In our analysis, we stress that we do not marginalize over the sound horizon in the EFTBOSS analysis. We do not expect that removing part of the data through the marginalization procedure would make BOSS data appear in strong tension with SH0ES, at least in EDE. Rather, we expect that constraints would significantly weaken. We leave for future work to test whether the determination of h from  $k_{eq}$  is robust to changes in the cosmological model.

When combining with Planck TTTEEE, we find that constraints on EDE are increased by ~5% with respect to the analogous analysis with Pantheon18, with  $f_{\rm EDE}(z_c) < 0.079$ . This can be understood by noting that the larger  $\Omega_m$  favored by Pantheon+, coupled with the positive correlation between  $f_{\rm EDE}(z_c) - h$ , can lead to high

 $<sup>^{24}</sup>$ More precisely, in Refs. [39,126,151], the marginalization over the sound horizon information is intended as a consistency test to be performed within  $\Lambda CDM$ .

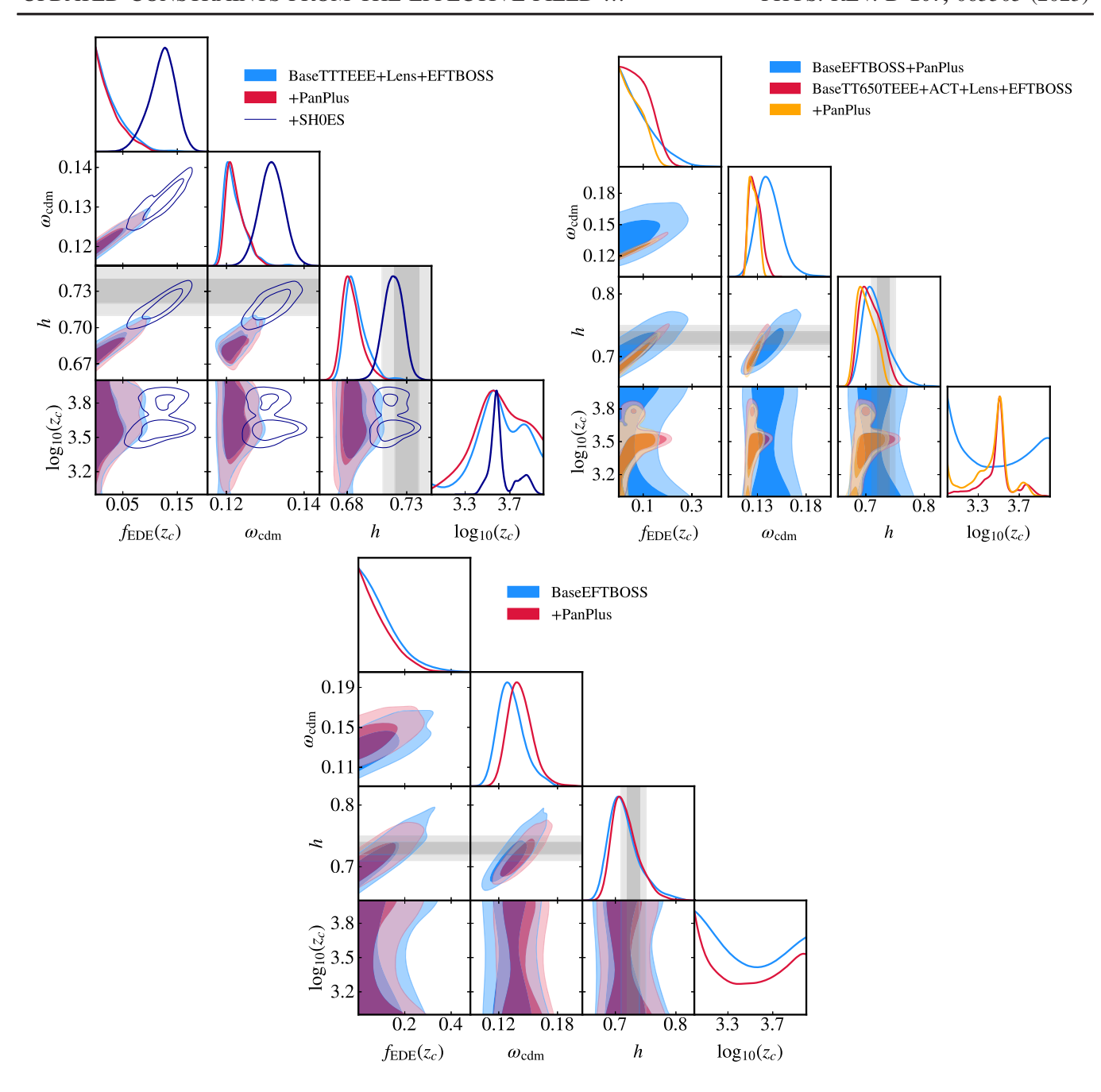


FIG. 7. Top left: 2D posterior distributions from BaseTTTEEE + Lens + EFTBOSS in combination with either Pantheon18 or Pantheon+ data, and the SH0ES Cepheid calibration. We recall that BaseTTTEEE refers to Planck TTTEEE + BAO + Pan18 data. Top right: 2D posterior distributions from BaseEFTBOSS and BaseTT650TEEE + ACT + Lens + EFTBOSS, in combination with either Pantheon18 or Pantheon+ data. We recall that BaseTT650TEEE refers to Planck TT650TEEE + BAO + Pan18 data, while BaseEFTBOSS refers to EFTBOSS + BBN + Lens + BAO + Pan18. Bottom: 2D posterior distributions from BaseEFTBOSS, with either Pantheon18 or Pantheon+ data.

 $\omega_m = \Omega_m h^2$  which are constrained by CMB data. However, once the SH0ES Cepheid calibration of SNIa is included, we find a strong preference for EDE, with  $f_{\rm EDE}(z_c) = 0.123^{+0.030}_{-0.018}$  (i.e., nonzero at more than  $5\sigma$ ) and a  $\Delta\chi^2({\rm EDE} - \Lambda{\rm CDM}) = -32.3$  (compared to -22.7 with Pantheon18). The cost in  $\chi^2$  for Planck TTTEEE + Lens and EFTBOSS compared to the analysis without the

SH0ES calibration is small, with  $\chi^2(\text{Planck})$  increasing by +2.3 and  $\chi^2(\text{EFTBOSS})$  increasing by +0.9, which further attests to the non-Gaussianity of the posterior in the absence of the SH0ES calibration. The  $Q_{\text{DMAP}}$  tension metric introduced earlier cannot be used as easily, due to the fact that the SH0ES data are now modeled in a more involved way, making use of a correlation matrix

connecting SNIa calibrators and high z SNIa [2], rather than the simple Gaussian prior on h.

Finally, when combining with Planck TT650TEEE and ACT, we find that the preference for EDE seen within ACT data further decreases to  $\Delta\chi^2 = -9.2$  (2.2 $\sigma$ ) and we derive a limit  $f_{\rm EDE}(z_c) < 0.137$ , with  $h = 0.700^{+0.013}_{-0.019}$  and a  $\lesssim 2\sigma$  tension with SH0ES. We defer to future work to further test the ability of EDE (and other promising models) to resolve the Hubble tension in light of this new Pantheon+ SNIa catalog.

#### V. DISCUSSION AND CONCLUSIONS

The developments of the predictions for the galaxy clustering statistics from the EFTofLSS have made possible the study of BOSS data beyond the conventional analyses dedicated to extracting BAO and  $f\sigma_8$  information. There has been in the recent literature a number of studies aiming at measuring the ACDM parameters at precision comparable with that of Planck CMB data (see, e.g., Refs. [38,39,98–102,104]). Additionally, it was shown that BOSS full-shape data, when analyzed using the one-loop predictions from the EFTofLSS (here called EFTBOSS data), can lead to strong constraints on extension to the ACDM model. In particular, the EDE model, currently one of the most promising models to resolve the Hubble tension [48,61], was shown to be severely constrained by EFTBOSS data [118,119]. However, it was subsequently argued that part of the constraints may come from a mismatch in the primordial power spectrum  $A_s$  amplitude between EFTBOSS and Planck [120].

Recently, it was found that the original EFTBOSS data used in these analyses were affected by an inconsistency between the normalization of the survey window function and the one of the data measurements, which led to a mismatch in  $A_s$ . A proper reanalysis of the EFTBOSS data constraints on the EDE model was lacking until now.

In this paper, we have performed a thorough investigation of the constraints on EDE in light of the correctly normalized EFTBOSS data and estimated the shifts introduced on the reconstructed cosmological parameters and their errors between various analysis strategies. A similar analysis within the  $\Lambda$ CDM model is presented in Sec. IV of our companion paper [108]. Our results are summarized in the following.

#### A. EFTBOSS constraints on EDE alone

We have shown in Sec. III B that, regardless of the BOSS data or the likelihood we consider, the BOSS full shape (analyzed on their own with a BBN prior) leads to reconstructed values of  $H_0$  that are compatible with what is obtained by the SH0ES Collaboration. Yet, the various EFTBOSS measurements, as well as the PyBird and CLASS-PT likelihoods, do not have the same constraining power on EDE:

- (i) When using the PyBird likelihood, we found  $f_{\rm EDE}(z_c) < 0.321$  when analyzing  $P_{\rm FKP}^{\rm LZ/CM} + \alpha_{\rm rec}^{\rm LZ/CM}$ , while analyzing  $P_{\rm QUAD}^{z_1/z_3} + \alpha_{\rm rec}^{z_1/z_3}$  yields  $f_{\rm EDE}(z_c) < 0.382$ , a ~20% difference.
- (ii) When using the same BOSS data, namely,  $P_{\text{QUAD}}^{z_1/z_3}$ , we have found that the PyBird likelihood gives  $f_{\text{EDE}}(z_c) < 0.382$ , while the CLASS-PT likelihood gives  $f_{\text{EDE}}(z_c) < 0.448$ , i.e., a ~15% difference.
- (iii) Restricting our analysis to the range of critical redshift  $\log_{10}(z_c) \in [3.4, 3.7]$  that can resolve the Hubble tension, we have shown that the combination of EFTBOSS+BBN+Lens+BAO+Pan18, leads to the constraints  $f_{\rm EDE}(z_c) < 0.2$  (95% C.L.) and  $h = 0.710^{+0.015}_{-0.025}$ , which does not exclude the EDE models resolving the Hubble tension.
- (iv) The inclusion of the recent Pantheon+ data does not affect this conclusion, as we find  $h = 0.717^{+0.015}_{-0.026}$ . We do not expect that marginalizing over the sound horizon as done in Refs. [39,126,151] would alter our conclusions, as it would simply remove information from the data. This question will be thoroughly explored elsewhere.

#### B. Planck + EFTBOSS constraints on EDE

In combination with Planck TTTEEE data, we have shown that constraints on EDE have changed due to the correction of the normalization of the window function:

- (i) The combination of Planck TTTEEE + Lens + BAO + Pan18 + EFTBOSS leads to  $f_{\rm EDE}(z_c) < 0.083$ , which is a ~10% improvement over the constraints without BOSS data and a ~5% improvement over the constraints with conventional BAO/ $f\sigma_8$  data. Yet, this is much weaker than the constraints reported with the incorrect normalization, namely,  $f_{\rm EDE} < 0.054$ . We quantify that the Hubble tension is reduced to the  $2.1\sigma$  level in the EDE cosmology (1.9 $\sigma$  without EFTBOSS) compared to 4.8 $\sigma$  in the  $\Lambda$ CDM model, and we find  $f_{\rm EDE}(z_c) = 0.103^{+0.027}_{-0.023}$  at  $z_c = 3970^{+255}_{-205}$  when the SH0ES prior is included.
- (ii) Replacing Pantheon18 by the new Pantheon+ data improves the constraints on EDE to  $f_{\rm EDE}(z_c) < 0.079$ . Yet, the inclusion of the SH0ES Cepheid calibration leads to  $f_{\rm EDE}(z_c) = 0.123^{+0.030}_{-0.018}$  at  $z_c = 4365^{+3000}_{-1100}$ , i.e., a nonzero  $f_{\rm EDE}(z_c)$  at more than  $5\sigma$  with  $\Delta\chi^2({\rm EDE}-\Lambda{\rm CDM})=-32.3$ . The cost in  $\chi^2$  for PlanckTTTEEE + Lens and EFTBOSS compared to the analysis without the SH0ES calibration is small, with  $\chi^2({\rm Planck})$  increasing by +2.3 and  $\chi^2({\rm EFTBOSS})$  increasing by +0.9, which attests of the non-Gaussianity of the posterior in the absence of the SH0ES calibration. This deserves to be studied further through a profile likelihood approach [123,124].

#### C. ACT + EFTBOSS constraints on EDE

Finally, we have studied the impact of EFTBOSS data on the recent hints of EDE observed within ACT DR4 data:

- (i) EFTBOSS reduces the preference for EDE over  $\Lambda$ CDM seen when analyzing ACT DR4, alone or in combination with restricted Planck TT data. The combination of Planck TT650TEEE + Lens + BAO + Pan18 + ACT + EFTBOSS leads to a mild constraints on  $f_{\rm EDE}(z_c) < 0.172$  with  $\Delta \chi^2({\rm EDE} \Lambda{\rm CDM}) = -11.1$ , to be compared with  $f_{\rm EDE}(z_c) = 0.128^{+0.064}_{-0.039}$  without EFTBOSS + Lens, with  $\Delta \chi^2({\rm EDE} \Lambda{\rm CDM}) = -14.6$ .
- (ii) The inclusion of Pantheon+ data further restricts  $f_{\text{EDE}}(z_c) < 0.137$ , with  $\Delta \chi^2(\text{EDE}-\Lambda\text{CDM}) = -9.2$ .
- (iii) When full Planck data are included, we derived a constraint  $f_{\rm EDE}(z_c) < 0.110$ , which is ~30% weaker than without ACT data. When all CMB data are included in combination with EFTBOSS, the Hubble tension is reduced to  $1.5\sigma$  in the EDE model, to be compared with  $4.7\sigma$  in  $\Lambda$ CDM. The inclusion of the SH0ES prior leads to  $f_{\rm EDE}(z_c) = 0.108^{+0.028}_{-0.021}$  at  $z_c = 3565^{+220}_{-495}$ .

We conclude that EFTBOSS data do not exclude EDE as a resolution to the Hubble tension, where we consistently find  $f_{\rm EDE}(z_c) \sim 10$ –12% at  $z_c \sim 3500$ –4000, with  $h \sim 0.72$ , when the Cepheid calibration is included in the analyses. However, EFTBOSS data do constrain very high EDE fraction as seen when analyzing ACT DR4 data.

#### **D.** Final comments

There are a number of relevant caveats to stress regarding our analyses. First, we note that the reconstructed  $S_8$  values from the various analyses that favor EDE are  $\sim 2.8-3.2\sigma$ higher than those coming from weak lensing measurement (and their cross-correlation with galaxy clustering) such as DES [35] and KiDS [34]. As was already pointed out in the past, this indicates that weak lensing data (and the existence of a  $S_8$  tension) could be used to further restrict the existence of EDE. Nevertheless, it has been noted that solutions to the  $S_8$  tension may be due to systematic effects [42] or nonlinear modeling including the effect of baryons at very small scales [41] or to a more complete dynamics in the dark sector [160,161]. In fact, models that resolve the  $S_8$ tension leave the EDE resolution unaffected [162,163] such that, although perhaps theoretically unappealing, it is possible that solutions to the  $H_0$  and  $S_8$  lie in different sectors. We leave for future work a robust study of EDE in light of the combination of EFTBOSS and weak lensing data, which will require better handling of the modeling of physical effects at scales beyond the range of validity of our EFT. Second, it will be very important to extend this work to include the bispectrum, which was recently analyzed at the one-loop level within  $\Lambda$ CDM [40,164]. It will also be interesting to see if the eBOSS surveys can shed light on EDE [165]: although the inclusion of eBOSS BAO was shown to not significantly modify the constraints on EDE (see, e.g., Refs. [48,119]), the analysis of the full-shape of eBOSS quasars may have the potential to put stronger limits given the large size of the survey. Additional constraints on EDE may also arise from measurements of the age of old objects such as globular clusters of stars [166,167], or the halo mass function at high z [168]. Interestingly, using N-body simulations, Ref. [168] showed that EDE predicts 50% more massive clusters at z=1 and twice more galaxy-mass halos at z=4 than  $\Lambda$ CDM. These predictions can be tested by observations from the James Webb Space Telescope and the first publicly available data are, in part, better fit by EDE than  $\Lambda$ CDM [169].

To close this work, we mention that we find here in agreement with previous literature, that the cosmological data including SH0ES prefer a higher value for the spectral tilt  $n_s$  in the EDE model than in  $\Lambda$ CDM, with  $n_s \sim 1$ allowed at  $\lesssim 2\sigma$  depending on the combination of data considered. Of interest here, we see that the inclusion of EFTBOSS data does not significantly pull back  $n_s$  to lower value, and when analyzed alone (with a BBN prior) also independently favors a value of  $n_s$  consistent with scale independence at  $\sim 1\sigma$ . A value of  $n_s$  close to that of the Harrison-Zeldovich spectrum, when put in perspective of CMB measurements of the tensor-to-scalar ratio, would dramatically change the status of the preferred inflationary models [170] (see also Refs. [171–173]). Therefore, if EDE is firmly detected with future cosmological data, beyond serving as resolution of the  $H_0$  tension, it would also have important consequences for early Universe physics.

#### ACKNOWLEDGMENTS

We thank Adam Riess for interesting discussions and comments at various stages of the project, as well as kindly sharing Pantheon+ and SH0ES data, and Dillon Brout and Dan Scolnic for their precious help with the implementation of the likelihood into MONTE PYTHON. We thank Guillermo Franco Abellán and José Louis Bernal for their contribution in the early stages of this project, and Guido D'Amico, Arnaud de Mattia, and Kevin Pardede for useful discussions. P. Z. would like to thank the organizers of the workshop "LSS2022: Recent Developments in Theoretical Large-Scale Structure—IFPU" for hospitality in Trieste during the late stage of completion of this project. This work has been partly supported by the CNRS-IN2P3 Grant No. Dark21. The authors acknowledge the use of computational resources from the Excellence Initiative of Aix-Marseille University (A\*MIDEX) of the "Investissements d'Avenir" program. These results have also been made possible thanks to LUPM's cloud computing infrastructure founded by Ocevu labex, and France-Grilles. This project has received support from the European Union's Horizon 2020 research and innovation program under the Marie Sklodowska-Curie Grant Agreement No. 860881-HIDDeN. This work used the Strelka Computing Cluster, which is run by Swarthmore College. T. L. S. is supported by NSF Grant No. 2009377, NASA Grant No. 80NSSC18K0728, and the Research Corporation.

## APPENDIX A: WINDOW FUNCTION NORMALIZATION

As discussed in Refs. [150,174,175] (see also [176]), the window function measurements, which are required to make an accurate theoretical calculation, have to be consistently normalized with the power spectrum measurements. The estimator for the power spectrum we are concerned with is the Feldman, Kaiser and Peacock (FKP) estimator [177], later generalized to redshift space in Refs. [178,179]. For fast estimation using FFTs [180,181], the line of sight for a given galaxy pair is chosen to be in the direction of one of galaxy in the pair,  $r_1$ . For clarity in the discussion we are going to have next, let us first gather here pieces of derivations that can be found partially in Refs. [98,182]. It is easy to see that the expectation value of the power spectrum FKP estimator reads (see, e.g., [183])

$$\langle \hat{P}_{\ell}(k) \rangle = \frac{2\ell + 1}{N_P} \int \frac{d\Omega_k}{4\pi} d^3 r_1 d^3 s e^{-ik \cdot s} \Theta(\mathbf{r}_1) \Theta(\mathbf{r}_1 + s) \times \bar{n}_w(\mathbf{r}_1) \bar{n}_w(\mathbf{r}_1 + s) \xi(s, \mathbf{r}_1) \mathcal{L}_{\ell}(\hat{k} \cdot \hat{r}_1), \tag{A1}$$

where  $\mathcal{L}_{\ell}$  is the Legendre polynomial of order  $\ell$ . Here  $\bar{n}_w(r) \equiv w(r)\bar{n}(r)$  is the weighted mean galaxy density, with weight w(r) being the FKP weights times some correction weights (usually to account for veto and instrumental/observational systematics),  $\Theta(r)$  is one if the galaxy at position r falls inside the survey, zero otherwise, and  $\xi(s,r_1)$  is the correlation function, with s the separation between two galaxies. Importantly,  $N_P$  is a normalization factor that is chosen by the user (see below). Using the following identity:

$$\int \frac{d\Omega_k}{4\pi} e^{-i\mathbf{k}\cdot\mathbf{s}} \mathcal{L}_{\ell}(\hat{\mathbf{k}}\cdot\hat{\mathbf{r}}_1) = (-i)^{\ell} j_{\ell}(\mathbf{k}\mathbf{s}) \mathcal{L}_{\ell}(\hat{\mathbf{s}}\cdot\hat{\mathbf{r}}_1), \quad (A2)$$

where  $j_\ell$  is the spherical-Bessel function of order  $\ell$ , we obtain

$$\langle \hat{P}_{\ell}(k) \rangle = \frac{(2\ell+1)}{N_P} (-i)^{\ell} \int ds \, s^2 j_{\ell}(ks) \int d\Omega_s$$

$$\times \int d^3 r_1 \Theta(\mathbf{r}_1) \Theta(\mathbf{r}_1 + \mathbf{s}) \bar{n}_w(\mathbf{r}_1) \bar{n}_w(\mathbf{r}_1 + \mathbf{s})$$

$$\times \xi(\mathbf{s}, \mathbf{r}_1) \mathcal{L}_{\ell}(\mu), \tag{A3}$$

where we have introduced the notation  $\mu \equiv \hat{s} \cdot \hat{r}_1$ . We now make the following approximation. We assume that the redshift evolution of the correlation function can be neglected within the observational bin such that

 $\xi(s, \mathbf{r}_1) \equiv \xi(s, \mu, r_1(z)) \simeq \xi(s, \mu, z_{\text{eff}}) \equiv \xi(s, \mu)$ , where the latter is evaluated at the effective redshift  $z_{\text{eff}}$  of the survey. <sup>25</sup> As such, we can pull out  $\xi(s, \mu)$  from the integral over  $d^3r_1$ . We can further expand in multipoles  $\xi(s, \mu) = \sum_{\ell'} \xi_{\ell'}(s) \mathcal{L}_{\ell'}(\mu)$  to pull out  $\xi_{\ell'}(s)$  from the angular integrals. Then, using the identity

$$\mathcal{L}_{\ell}(\mu)\mathcal{L}_{\ell'}(\mu) = \sum_{L} \begin{pmatrix} \ell & L & \ell' \\ 0 & 0 & 0 \end{pmatrix}^{2} (2L+1)\mathcal{L}_{L}(\mu), \quad (A4)$$

where  $\begin{pmatrix} \ell & L \ell' \\ 0 & 0 & 0 \end{pmatrix}$  are the Wigner 3-j symbols, we get

$$\langle \hat{P}_{\ell}(k) \rangle = 4\pi (2\ell + 1)(-i)^{\ell} \sum_{\ell', L} \begin{pmatrix} \ell' & L & \ell' \\ 0 & 0 & 0 \end{pmatrix}^{2}$$

$$\times \int ds \, s^{2} j_{\ell}(ks) \xi_{\ell'}(s) Q_{L}(s), \tag{A5}$$

where we have defined the window functions

$$Q_L(s) \equiv \frac{(2L+1)}{N_P} \int \frac{d\Omega_s}{4\pi} \int d^3r_1 \Theta(\mathbf{r}_1) \Theta(\mathbf{r}_1 + s) \times \bar{n}_w(\mathbf{r}_1) \bar{n}_w(\mathbf{r}_1 + s) \mathcal{L}_L(\mu). \tag{A6}$$

Inserting the relation between the multipoles of the correlation function and those of the power spectrum,

$$\xi_{\ell'}(s) = i^{\ell'} \int \frac{dk'}{2\pi^2} k'^2 P_{\ell'}(k') j_{\ell'}(k's),$$
 (A7)

we finally obtain

$$\langle \hat{P}_{\ell}(k) \rangle = \int dk' \, k'^2 \sum_{\ell'} W_{\ell\ell'}(k, k') P_{\ell'}(k'), \quad (A8)$$

where we have defined

$$W_{\ell,\ell'}(k,k') = \frac{2}{\pi} (2\ell+1)(-i)^{\ell} i^{\ell'} \int ds \, s^2 j_{\ell}(ks) j_{\ell'}(k's) \times \sum_{l} {\ell \choose 0 \quad 0 \quad 0}^2 Q_L(s). \tag{A9}$$

Notice that, for clarity, we have neglected the integral constraints [174], as well as wide-angle contributions [182]. Our master formula is Eq. (A8): to predict the observed power spectrum  $\langle \hat{P}_{\ell'}(k) \rangle$ , we simply need to convolve our predictions  $P_{\ell'}(k')$  with  $W_{\ell,\ell'}(k,k')$  given by Eq. (A9).  $W_{\ell,\ell'}(k,k')$  can be precomputed, and the only input we need is  $Q_L(s)$ .

<sup>&</sup>lt;sup>25</sup>See Ref. [183] for a BOSS analysis that does not rely on this approximation.

<sup>&</sup>lt;sup>26</sup>We have checked that neglecting the integral constraints in the BOSS full-shape analysis leads to small shifts in the posteriors of  $\lesssim 1/4 \cdot \sigma$ .

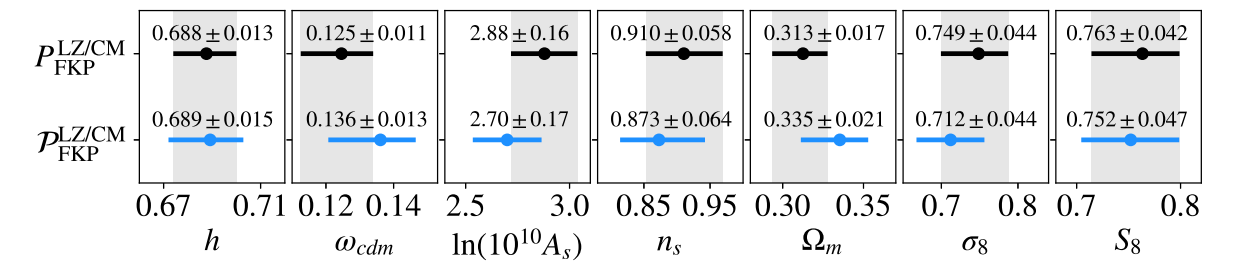


FIG. 8. Comparison of  $\Lambda$ CDM results from BOSS full-shape analysis of the power spectrum measurements  $\mathcal{P}_{FKP}^{LZ/CM}$  and  $P_{FKP}^{LZ/CM}$ , analyzed with window functions inconsistently and consistently normalized, respectively (see Table I). The gray bands are centered on the results from the  $P_{FKP}^{LZ/CM}$  data.

The window function  $Q_L(s)$ , Eq. (A6), can be obtained in the following way [182]. Using Eq. (A7) and the identity

$$\int dk \frac{(ks)^2}{2\pi^2} j_L(ks) j_L(ks') = \frac{1}{4\pi} \delta_D(s - s'), \quad (A10)$$

where  $\delta_D$  is the Dirac delta distribution, we see that

$$Q_L(s) = i^L \int \frac{dk}{2\pi^2} k^2 \mathcal{Q}_L(k) j_L(ks), \qquad (A11)$$

where  $Q_L(k)$  is the expectation value of a power spectrum as defined in Eq. (A3) given  $\xi(s, r_1) \equiv 1$ . Therefore,  $Q_L(k)$  can be measured as the power spectrum  $P_L^r(k)$  of random objects (whose distribution is approaching Poisson) within the same geometry survey that we are dealing with,

$$Q_L(k) \equiv \alpha \langle \hat{P}_L^r(k) \rangle,$$
 (A12)

where  $\alpha = N_g/N_r$  is the ratio of the number of data "galaxy" objects to the number of random objects. Such catalog of random objects is already available to us, as it is also required for the estimation of the power spectrum.

The key point is the following:  $\mathcal{Q}_L(k)$  is normalized by the same normalization factor as  $P_\ell(k)$ , namely,  $N_P$ . As such, in the limit of vanishing separation  $s \to 0$ , the window function monopole does not go to unity,  $Q_0(s) \neq 1$ , but instead

$$Q_0(s \to 0) \to \frac{1}{N_P} \int d^3 r_1 \bar{n}_w^2(\mathbf{r}).$$
 (A13)

Given that one does not know the value of the numerator in the equation above prior to making the measurement,  $N_P$  can only be estimated *approximately* in order to have  $Q_0(s)$  approaching 1 at vanishing separation  $s \to 0$ . It is in this sense that  $N_P$  is chosen by the user. However, the normalization choice is not important as long as the window function measurements are consistently normalized with the power spectrum measurements. Given the measurement protocol

sketched above, this is automatic if one is able to evaluate (A11) accurately.<sup>27</sup>

In past BOSS full-shape analyses, e.g., [98–100,118,119], the window function normalizations were instead inconsistently enforced to  $Q_0^{\text{wrong}}(0) \equiv 1$ , while in reality  $Q_0(0) \sim 0.9$  given the choice of  $N_P$ . Such inconsistency of  $\sim 0.9$  led to a shift in  $A_s$  of around  $-1\sigma$  depending on the normalization choice. Let us list two choices for the normalization factor  $N_P$ :

- (i) Choice 1:  $N_P = \alpha \sum_{\{i \in \text{randoms}\}} \bar{n}(r_i) w_{\text{FKP}}^2(r_i)$ . This was the choice in Ref. [184], which measurements were used in, e.g., Refs. [99,118].
- (ii) Choice 2:  $N_P = \mathcal{A} * \int dr \bar{n}_w^2(r)$ , where  $\bar{n}_w(r)$  is inferred from counting galaxies and binning them in shells and  $\mathcal{A}$  is an associated estimated area. This was the choice in Ref. [147], which measurements  $\mathcal{P}_{\text{FKP}}^{\text{LZ/CM}}$  were used in, e.g., Refs. [98,100,119].  $\mathcal{P}_{\text{FKP}}^{\text{LZ/CM}}$ , as defined in Table I, is assigned window functions that are inconsistently normalized.

We stress again that those choices are not important as long as the same  $N_P$  is used to normalize the window functions and

<sup>28</sup>Naively one might think that the sum over enough objects is a good approximation to the volume integral; Actually, choice 1 poorly estimates the integral in Eq. (A13) because in the FKP estimator,  $\bar{n}$  is measured from the grid for FFT with finite cell resolution, while in choice 1, we are counting the objects instead.

<sup>29</sup>We thank Hector Gil-Marín for private correspondence on this point.

At https://github.com/pierrexyz/fkpwin, we provide a code written to perform the window function measurements, based on NBODYKIT. Let us note that we find that it is not straightforward to get a precise measurements of  $\hat{Q}_L(k)$ , namely, the power spectrum of the random objects over the whole range of k for which  $\hat{Q}_L(k)$  contributes significantly to the integral in Eq. (A11). Furthermore, the estimator in Eq. (A12) might have a nonnegligible variance, given that only one catalog is used. We nevertheless have checked that, letting the normalization of the window functions to be different from the one of the power spectrum by a few percents leads to tolerable shifts in the posteriors ( $\lesssim 1\sigma/5$ ) inferred fitting BOSS data. For future large-volume datasets, it would be, however, desirable to have a better numerical control over the measurements of  $Q_L(s)$  such that the normalization consistency with  $P_{\ell}(k)$  is achieved to sufficient accuracy given increasing precision of the data.

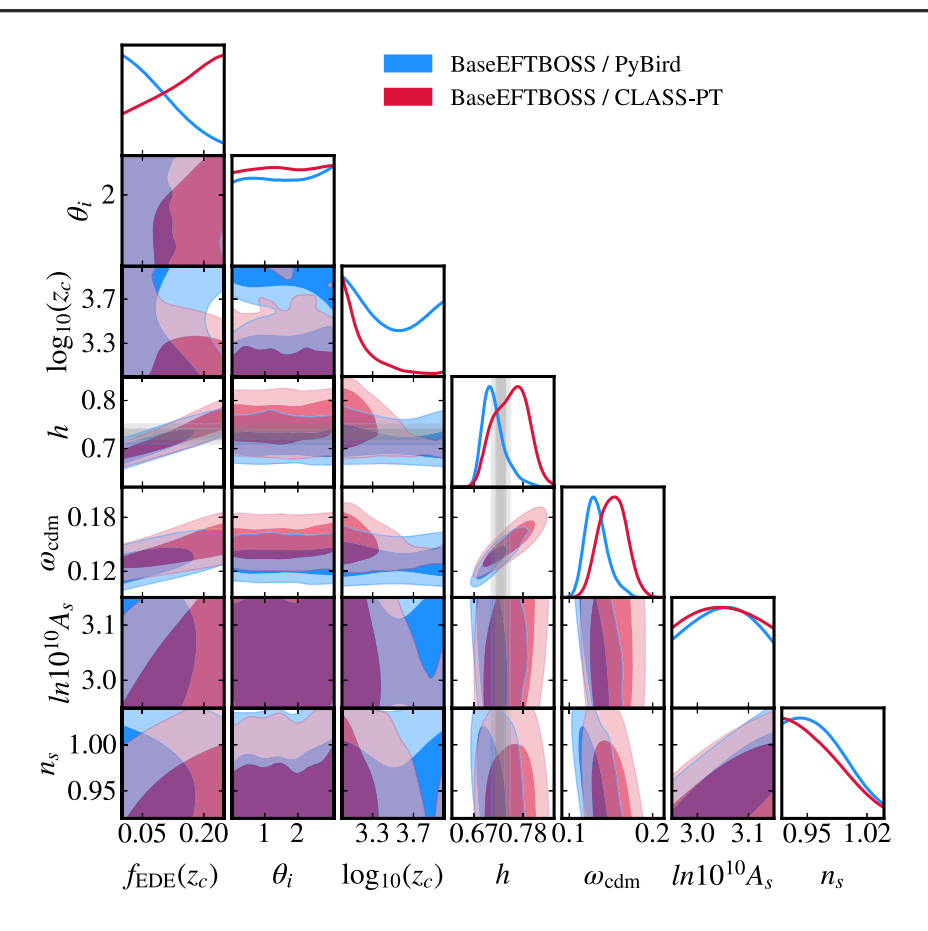


FIG. 9. Comparison between the 2D posterior distributions of a subset of parameters in the EDE model reconstructed from the PyBird or CLASS-PT likelihood, in combination with BBN + Lens + BAO + Pan18 (i.e., BaseEFTBOSS).

the power spectrum measurements. As already mentioned in the main text, except for  $\mathcal{P}_{FKP}^{LZ/CM}$  that is used in this paper for illustration purposes, all power spectrum measurements obtained with the FKP estimator, namely,  $P_{FKP}^{LZ/CM}$  and  $P_{FKP}^{z_1/z_3}$ , are instead consistently normalized with their window functions (see Table I for more details on the measurements). We finish this section by noting that, in analyses using measurements obtained from the FKP estimator, but also from the other estimators, the posteriors may depend on the effective-redshift approximation used above. This suggests that, for each estimator, more work is needed to understand the accuracy of this approximation, along the line of, e.g., [183] for the correlation function.

In Fig. 8, we show a comparison of the 1D posteriors from the full-shape analysis of the BOSS power spectrum measured with the FKP estimator, using window functions with consistent or inconsistent normalization. The inconsistency leads to a lower amplitude  $A_s$ , or equivalently  $\sigma_8$ , as well as higher  $\Omega_m \sim f$ , where f is the logarithmic growth rate, through anticorrelation. We find notable shifts on  $\omega_{\rm cdm}$ ,  $\ln(10^{10}A_s)$ ,  $\Omega_m$  and  $\sigma_8$  of  $0.9\sigma$ ,  $1.1\sigma$ ,  $1.1\sigma$ , and  $0.8\sigma$ , respectively.

#### APPENDIX B: ADDITIONAL COMPARISON BETWEEN THE PyBird AND CLASS-PT LIKELIHOOD IN EDE

In Figs. 9–11, we show the 2D posterior distributions reconstructed from BaseEFTBOSS, BaseTTTEEE + Lens + EFTBOSS, and BaseTT650TEEE+ACT+Lens + EFTBOSS, respectively, comparing the results from the PyBird and the CLASS-PT likelihoods. In addition, we recall that EFTBOSS corresponds to  $P_{\rm FKP}^{\rm LZ/CM} + \alpha_{\rm rec}^{z_1/z_3}$  in the framework of the PyBird likelihood and to  $P_{\rm QUAD}^{z_1/z_3} + \beta_{\rm rec}^{z_1/z_3}$  in the framework of the CLASS-PT likelihood (see Table I). The most striking differences occur in the BaseEFTBOSS alone case, for which CLASS-PT leads to much weaker constraints on  $f_{\rm EDE}(z_c)$  and much larger error bars on h and  $\omega_{\rm cdm}$ . The origin of these differences can be traced back to the discussion presented in our companion

<sup>&</sup>lt;sup>30</sup>For this comparison, LOWZ SGC is not included in the PyBird likelihood. As expected, we have checked that the addition of this sky cut does not change the posteriors for the corresponding analyses.

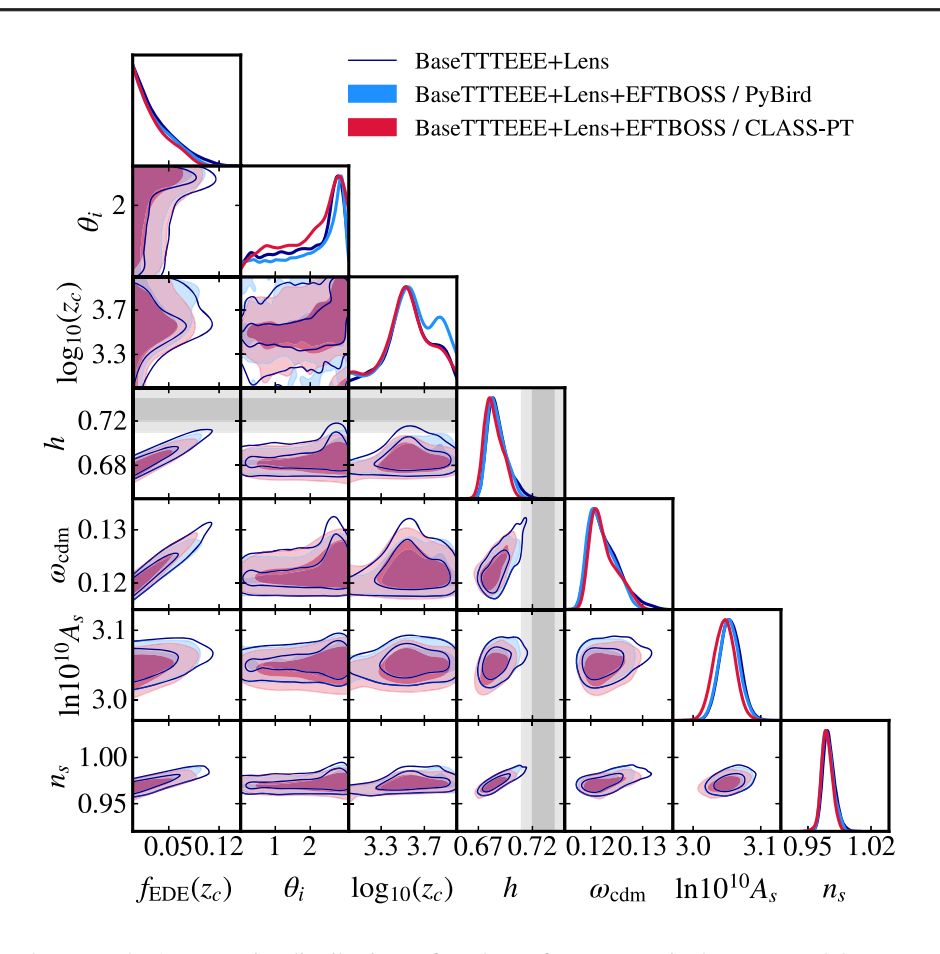


FIG. 10. Comparison between the 2D posterior distributions of a subset of parameters in the EDE model reconstructed from the PyBird or CLASS-PT likelihood, in combination with BaseTTTEEE + Lens.

paper [108], namely, to the choice of the power spectrum estimators, the BOSS post-reconstructed measurements used, the scale cut, the number of multipoles, and more importantly, the choice of EFT parameter priors. Once PlanckTTTEEE or PlanckTT650TEEE + ACT data are included in the analysis, we find that the reconstructed posteriors are very similar between the two EFTBOSS

implementations and mostly driven by CMB data. We conclude that the main results of this paper, drawn from the combination of CMB and LSS data, are unaffected by the choice of EFT implementation. However, parameter reconstruction based on EFTBOSS data alone may vary at the  $1\sigma$  level.

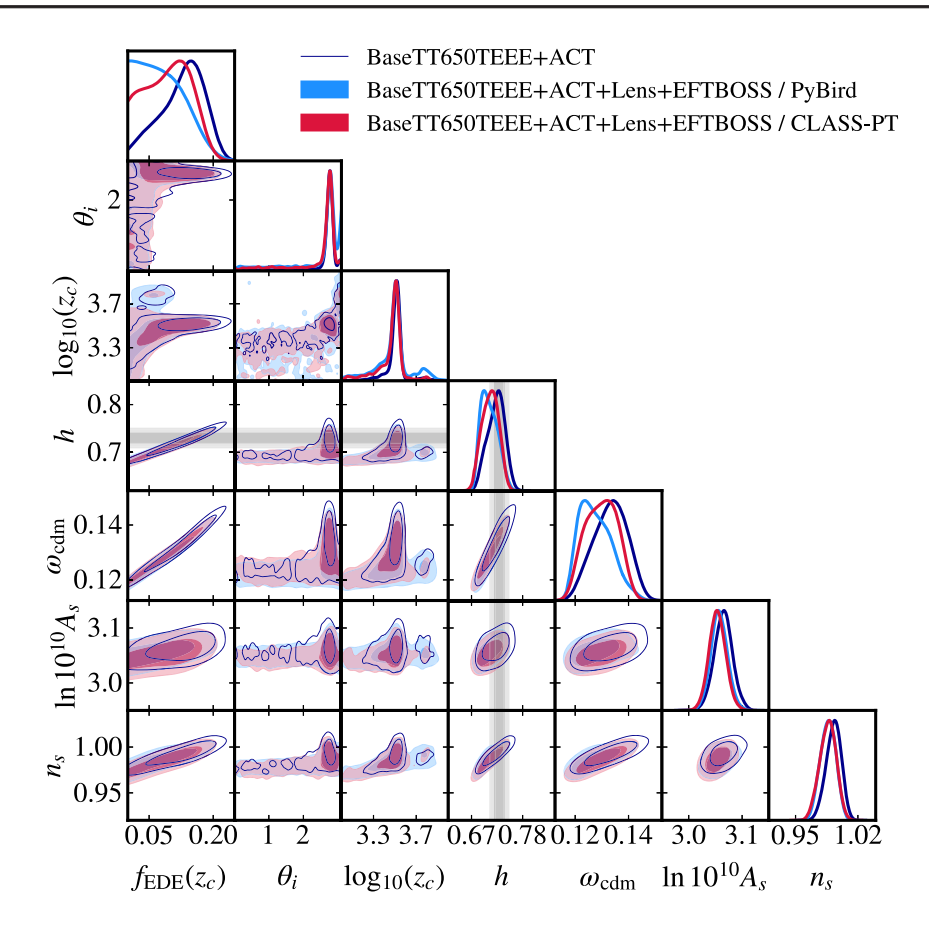


FIG. 11. Comparison between the 2D posterior distributions of a subset of parameters in the EDE model reconstructed from the PyBird or CLASS-PT likelihood, in combination with BaseTT650TEEE + ACT + Lens.

#### APPENDIX C: $\chi^2$ PER EXPERIMENT

In this appendix, we report the best-fit  $\chi^2$  per experiment for both  $\Lambda$ CDM and EDE models. In Tables VII and VIII

are presented the runs including Planck data, in Table IX the runs including ACT data, and in Table X the combination of the full Planck data and ACT data. Finally, Table XI present runs including the PanPlus data.

TABLE VII. Best-fit  $\chi^2$  per experiment (and total) for  $\Lambda$ CDM when fit to different data combinations: BaseTTTEEE + Lens, BaseTTTEEE + Lens +  $f\sigma_8$ , BaseTTTEEE + Lens + EFTBOSS, with and without SH0ES. We also report the tension metric  $Q_{\rm DMAP} \equiv \sqrt{\chi^2({\rm w/SH0ES}) - \chi^2({\rm w/o~SH0ES})}$ .

ACDM							
Planck high-ℓ TTTEEE	2342.2	2345.0	2342.2	2344.6	2342.2	2345.2	
Planck low-ℓ TT	23.4	22.9	23.5	23.0	23.4	22.8	
Planck low- $\ell$ EE	396.3	397.2	396.1	397.2	396.3	397.2	
Planck lensing	8.9	9.4	9.0	9.4	9.0	9.4	
BOSS BAO low $z$	1.2	1.9	1.2	1.8	1.2	1.9	
BOSS BAO DR12	4.3	3.4					
BOSS BAO/ $f\sigma_8$ DR12			6.7	5.9			
EFTBOSS CMASS					84.6	83.1	
EFTBOSS LOWZ					33.5	33.7	
Pantheon	1027.2	1026.9	1027.2	1026.9	1027.2	1026.9	
SH0ES	• • •	19.9		20.4		19.8	
Total $\chi^2_{\rm min}$	3803.6	3826.6	3805.7	3829.1	3917.4	3940.0	
$Q_{\mathrm{DMAP}}$	4.	8σ	4.	$8\sigma$	4.	$8\sigma$	

TABLE VIII. Best-fit  $\chi^2$  per experiment (and total) for EDE when fit to different data combinations: BaseTTTEEE + Lens, BaseTTTEEE + Lens +  $f\sigma_8$ , BaseTTTEEE + Lens + EFTBOSS, with and without SH0ES. We also report the  $\Delta\chi^2_{\rm min} \equiv \chi^2_{\rm min}({\rm EDE}) - \chi^2_{\rm min}(\Lambda{\rm CDM})$  and the tension metric  $Q_{\rm DMAP} \equiv \sqrt{\chi^2({\rm w/SH0ES}) - \chi^2({\rm w/o\,SH0ES})}$ .

		Е	DE			
Planck high-€ TTTEEE	2339.4	2341.5	2339.1	2340.9	2339.3	2341.1
Planck low-ℓ TT	21.8	20.4	22.0	20.6	21.1	20.5
Planck low- $\ell$ EE	396.4	396.8	396.1	396.4	396.1	396.9
Planck lensing	9.5	10.0	9.3	9.9	9.6	9.9
BOSS BAO low $z$	1.6	1.8	1.4	1.7	1.4	1.9
BOSS BAO DR12	3.7	3.5				
BOSS BAO/ $f\sigma_8$ DR12			6.5	7.0		
EFTBOSS CMASS					84.1	83.3
EFTBOSS LOWZ					34.0	34.4
Pantheon	1027.0	1026.9	1027.0	1026.9	1027.0	1026.9
SH0ES	• • •	2.0	• • •	3.2	• • •	2.3
Total $\chi^2_{\rm min}$	3799.2	3802.9	3801.8	3806.1	3912.7	3917.3
$\Delta \chi^2_{\min} (EDE - \Lambda CDM)$	-3.8	-23.7	-3.9	-23.0	-4.7	-22.7
Preference over ΛCDM	$1\sigma$	$4.2\sigma$	$1.1\sigma$	$4.1\sigma$	$1.3\sigma$	$4.1\sigma$
$Q_{\mathrm{DMAP}}$	1.	9σ	2.	0σ	2.	$1\sigma$

TABLE IX. Best-fit  $\chi^2$  per experiment (and total) for  $\Lambda$ CDM and EDE when fit to different data combinations: BaseTT650TEEE + ACT, BaseTT650TEEE + ACT +  $f\sigma_8$ , BaseTT650TEEE + ACT + EFTBOSS, BaseTT650TEEE + ACT + Lens + EFTBOSS, and BaseTT650TEEE + ACT + Lens + EFTBOSS + PanPlus. We also report the  $\Delta\chi^2_{\min} \equiv \chi^2_{\min}(\text{EDE}) - \chi^2_{\min}(\Lambda \text{CDM})$  and the corresponding preference over  $\Lambda$ CDM, computed assuming the  $\Delta\chi^2$  follows a  $\chi^2$  distribution with 3 degrees of freedom.

			ΛCDM					EDE		
Planck high-ℓ TT650TEEE	1843.5	1842.6	1842.9	1842.8	1842.6	1837.5	1838.0	1836.9	1836.8	1837.7
Planck low-ℓ TT	21.5	21.7	21.5	21.7	21.8	20.7	20.9	20.8	20.9	21.2
Planck low- $\ell$ EE	395.7	395.7	395.8	395.9		395.8	395.8	395.8	395.8	395.8
Planck lensing				9.0	9.0				10.2	9.9
ACT DR4	293.8	294.5	294.4	294.2	294.3	285.4	285.0	285.9	286.4	286.9
BOSS BAO low $z$	1.5	1.4	1.6	1.5	1.4	2.1	2.0	2.4	2.3	1.9
BOSS BAO DR12	3.7					3.5				
BOSS BAO/ $f\sigma_8$ DR12		6.1					7.2			
EFTBOSS CMASS			83.4	83.6	84.9			84.5	84.3	84.3
EFTBOSS LOWZ			33.7	33.7	33.7			35.1	34.7	34.4
Pantheon	1026.8	1027.0	1027.0	1027.0		1026.9	1026.9	1026.9	1026.9	
Pantheon+					1411.8		• • •	• • •	• • •	1413.0
Total $\chi^2_{\rm min}$	3586.5	3589.1	3700.3	3709.5	4094.3	3571.9	3575.8	3688.3	3698.4	4085.1
$\Delta \chi^2_{\rm min}({\rm EDE} - \Lambda {\rm CDM})$						-14.6	-13.3	-12.0	-11.1	-9.2
Preference over ΛCDM		• • •	• • •	• • •	• • •	$3.1\sigma$	$2.9\sigma$	$2.7\sigma$	$2.5\sigma$	$2.2\sigma$

TABLE X. Best-fit  $\chi^2$  per experiment (and total) for  $\Lambda$ CDM and EDE when fit to BaseTTTEEE+ ACT+Lens+EFTBOSS, with and without SH0ES. We also report the  $\Delta\chi^2_{\rm min}\equiv\chi^2_{\rm min}({\rm EDE})-\chi^2_{\rm min}(\Lambda{\rm CDM})$  and the tension metric  $Q_{\rm DMAP}\equiv\sqrt{\chi^2({\rm w/SH0ES})-\chi^2({\rm w/o\,SH0ES})}$ .

	ΛС	DM	Е	DE
Planck high-ℓ TTTEEE	2349.8	2352.0	2346.2	2347.2
Planck low-ℓ TT	22.4	22.0	21.9	21.2
Planck low- $\ell$ EE	396.2	396.8	396.1	396.4
Planck lensing	8.9	8.9	9.6	9.8

(Table continued)

TABLE X. (Continued)

	ΛС	DM	Е	DE
ACT DR4	240.6	241.0	236.8	236.2
BOSS BAO low $z$	1.4	2.0	1.7	2.2
EFTBOSS CMASS	84.1	82.9	84.2	84.2
EFTBOSS LOWZ	33.6	33.8	34.2	34.6
Pantheon	1027.1	1026.9	1026.9	1026.9
SH0ES	• • •	19.5	• • •	1.10
Total $\chi^2_{\rm min}$	4164.0	4185.9	4157.6	4159.8
$\Delta \chi^2_{\min}(\text{EDE} - \Lambda \text{CDM})$			-6.4	-26.1
Preference over ΛCDM			$1.7\sigma$	$4.4\sigma$
$Q_{ m DMAP}$	4.	$7\sigma$	1	$.5\sigma$

TABLE XI. Best-fit  $\chi^2$  per experiment (and total) for  $\Lambda$ CDM and EDE when fit to BaseTTTEEE + Lens + EFTBOSS + PanPlus, with and without SH0ES. We also report the  $\Delta\chi^2_{min} \equiv \chi^2_{min}(\text{EDE}) - \chi^2_{min}(\Lambda \text{CDM})$  and the corresponding preference over  $\Lambda$ CDM, computed assuming the  $\Delta\chi^2$  follows a  $\chi^2$  distribution with 3 degrees of freedom.

	ΛΟ	CDM	E	DE
Planck high-ℓ TTTEEE	2346.18	2349.5	2344.0	2346.9
Planck low-ℓ TT	23.0	22.4	22.3	21.0
Planck low-€ EE	396.1	397.7	396.3	396.3
Planck lensing	8.8	9.1	9.0	9.6
BOSS BAO low $z$	1.1	2.1	1.3	1.8
EFTBOSS CMASS	85.2	82.9	85.0	85.1
EFTBOSS LOWZ	33.6	33.8	33.8	34.6
Pantheon+	1411.1		1411.6	
Pantheon + SH0ES	• • •	1321.9		1291.6
Total $\chi^2_{\rm min}$	4305.1	4219.3	4303.2	4187.0
$\Delta \chi^2_{\min}(\text{EDE} - \Lambda \text{CDM})$			-1.9	-32.3
Preference over ΛCDM	•••	•••	$0.5\sigma$	5σ

- [1] N. Aghanim *et al.* (Planck Collaboration), Planck 2018 results. VI. Cosmological parameters, Astron. Astrophys. **641**, A6 (2020); **652**, C4(E) (2021).
- [2] Adam G. Riess *et al.*, A comprehensive measurement of the local value of the Hubble constant with 1 km s<sup>-1</sup> Mpc<sup>-1</sup> uncertainty from the Hubble space telescope and the SH0ES Team, Astrophys. J. Lett. **934**, L7 (2022).
- [3] Adam G. Riess, Louise Breuval, Wenlong Yuan, Stefano Casertano, Lucas M. Macri, Dan Scolnic, Tristan Cantat-Gaudin, Richard I. Anderson, and Mauricio Cruz Reyes, Cluster Cepheids with high precision Gaia parallaxes, low zero-point uncertainties, and Hubble space telescope photometry, Astrophys. J. 938, 36 (2022).
- [4] Maria Giovanna Dainotti, Biagio De Simone, Tiziano Schiavone, Giovanni Montani, Enrico Rinaldi, and Gaetano Lambiase, On the Hubble constant tension in

- the SNe Ia Pantheon sample, Astrophys. J. **912**, 150 (2021).
- [5] Maria Giovanna Dainotti, Biagio De Simone, Tiziano Schiavone, Giovanni Montani, Enrico Rinaldi, Gaetano Lambiase, Malgorzata Bogdan, and Sahil Ugale, On the evolution of the Hubble constant with the SNe Ia Pantheon sample and baryon acoustic oscillations: A feasibility study for GRB-cosmology in 2030, Galaxies 10, 24 (2022).
- [6] Edvard Mortsell, Ariel Goobar, Joel Johansson, and Suhail Dhawan, Sensitivity of the Hubble constant determination to Cepheid calibration, Astrophys. J. 933, 212 (2022).
- [7] Edvard Mortsell, Ariel Goobar, Joel Johansson, and Suhail Dhawan, The Hubble tension revisited: Additional local distance ladder uncertainties, Astrophys. J. 935, 58 (2022).
- [8] Brent Follin and Lloyd Knox, Insensitivity of the distance ladder Hubble constant determination to Cepheid

- calibration modelling choices, Mon. Not. R. Astron. Soc. 477, 4534 (2018).
- [9] M. Rigault *et al.*, Confirmation of a star formation bias in type Ia supernova distances and its effect on measurement of the Hubble constant, Astrophys. J. **802**, 20 (2015).
- [10] M. Rigault *et al.* (Nearby Supernova Factory Collaboration), Strong dependence of type Ia supernova standardization on the local specific star formation rate, Astron. Astrophys. 644, A176 (2020).
- [11] D. O. Jones *et al.*, Should type Ia supernova distances be corrected for their local environments?, Astrophys. J. 867, 108 (2018).
- [12] Dillon Brout and Daniel Scolnic, It's dust: Solving the mysteries of the intrinsic scatter and host-galaxy dependence of standardized type Ia supernova brightnesses, Astrophys. J. 909, 26 (2021).
- [13] G. E. Addison, Y. Huang, D. J. Watts, C. L. Bennett, M. Halpern, G. Hinshaw, and J. L. Weiland, Quantifying discordance in the 2015 Planck CMB spectrum, Astrophys. J. 818, 132 (2016).
- [14] N. Aghanim *et al.* (Planck Collaboration), Planck intermediate results. LI. Features in the cosmic microwave background temperature power spectrum and shifts in cosmological parameters, Astron. Astrophys. 607, A95 (2017).
- [15] Eleonora Di Valentino, Alessandro Melchiorri, and Joseph Silk, Planck evidence for a closed universe and a possible crisis for cosmology, Nat. Astron. **4**, 196 (2019).
- [16] Will Handley, Curvature tension: Evidence for a closed universe, Phys. Rev. D 103, L041301 (2021).
- [17] Nils Schöneberg, Julien Lesgourgues, and Deanna C. Hooper, The BAO + BBN take on the Hubble tension, J. Cosmol. Astropart. Phys. 10 (2019) 029.
- [18] G. E. Addison, D. J. Watts, C. L. Bennett, M. Halpern, G. Hinshaw, and J. L. Weiland, Elucidating ΛCDM: Impact of baryon acoustic oscillation measurements on the Hubble constant discrepancy, Astrophys. J. 853, 119 (2018).
- [19] Wendy L. Freedman, Barry F. Madore, Dylan Hatt, Taylor J. Hoyt, In Sung Jang, Rachael L. Beaton, Christopher R. Burns, Myung Gyoon Lee, Andrew J. Monson, Jillian R. Neeley, M. M. Phillips, Jeffrey A. Rich, and Mark Seibert, The Carnegie-Chicago Hubble program. VIII. An independent determination of the Hubble constant based on the tip of the red giant branch, Astrophys. J. 882, 34 (2019).
- [20] Wendy L. Freedman, Measurements of the Hubble constant: Tensions in perspective, Astrophys. J. 919, 16 (2021).
- [21] Gagandeep S. Anand, R. Brent Tully, Luca Rizzi, Adam G. Riess, and Wenlong Yuan, Comparing tip of the red giant branch distance scales: An independent reduction of the Carnegie-Chicago Hubble program and the value of the Hubble constant, Astrophys. J. 932, 15 (2022).
- [22] Wenlong Yuan, Adam G. Riess, Lucas M. Macri, Stefano Casertano, and Dan Scolnic, Consistent calibration of the tip of the red giant branch in the large Magellanic cloud on the Hubble space telescope photometric system and implications for the determination of the Hubble constant, Astrophys. J. 886, 61 (2019).
- [23] John Soltis, Stefano Casertano, and Adam G. Riess, The parallax of  $\omega$  centauri measured from Gaia EDR3 and a

- direct, geometric calibration of the tip of the red giant branch and the Hubble constant, Astrophys. J. Lett. **908**, L5 (2021).
- [24] Nandita Khetan *et al.*, A new measurement of the Hubble constant using type Ia supernovae calibrated with surface brightness fluctuations, Astron. Astrophys. **647**, A72 (2021).
- [25] Caroline D. Huang, Adam G. Riess, Wenlong Yuan, Lucas M. Macri, Nadia L. Zakamska, Stefano Casertano, Patricia A. Whitelock, Samantha L. Hoffmann, Alexei V. Filippenko, and Daniel Scolnic, Hubble space telescope observations of Mira variables in the Type Ia supernova host NGC 1559: An alternative candle to measure the Hubble constant, Astrophys. J. 889, 5 (2020).
- [26] James Schombert, Stacy McGaugh, and Federico Lelli, Using the baryonic Tully-Fisher relation to measure  $H_o$ , Astrophys. J. **160**, 71 (2020).
- [27] Kenneth C. Wong *et al.*, H0LiCOW—XIII. A 2.4 per cent measurement of  $H_0$  from lensed quasars:  $5.3\sigma$  tension between early- and late-Universe probes, Mon. Not. R. Astron. Soc. **498**, 1420 (2020).
- [28] S. Birrer *et al.*, TDCOSMO—IV. Hierarchical time-delay cosmography—joint inference of the Hubble constant and galaxy density profiles, Astron. Astrophys. **643**, A165 (2020).
- [29] D. W. Pesce *et al.*, The Megamaser Cosmology Project. XIII. Combined Hubble constant constraints, Astrophys. J. Lett. **891**, L1 (2020).
- [30] B. P. Abbott *et al.* (LIGO Scientific and Virgo Collaborations), A gravitational-wave measurement of the Hubble constant following the second observing run of Advanced LIGO and Virgo, Astrophys. J. **909**, 218 (2021).
- [31] Eleonora Di Valentino, Olga Mena, Supriya Pan, Luca Visinelli, Weiqiang Yang, Alessandro Melchiorri, David F. Mota, Adam G. Riess, and Joseph Silk, In the realm of the Hubble tension—a review of solutions, Classical Quantum Gravity 38, 153001 (2021).
- [32] Elcio Abdalla *et al.*, Cosmology intertwined: A review of the particle physics, astrophysics, and cosmology associated with the cosmological tensions and anomalies, J. High Energy Astrophys. **34**, 49 (2022).
- [33] Catherine Heymans *et al.*, CFHTLenS: The Canada-France-Hawaii telescope lensing survey, Mon. Not. R. Astron. Soc. **427**, 146 (2012).
- [34] Catherine Heymans *et al.*, KiDS-1000 Cosmology: Multi-probe weak gravitational lensing and spectroscopic galaxy clustering constraints, Astron. Astrophys. **646**, A140 (2021).
- [35] T. M. C. Abbott *et al.* (DES Collaboration), Dark Energy Survey Year 3 results: Cosmological constraints from galaxy clustering and weak lensing, Phys. Rev. D 105, 023520 (2022).
- [36] P. A. R. Ade *et al.* (Planck Collaboration), Planck 2015 results. XXIV. Cosmology from Sunyaev-Zeldovich cluster counts, Astron. Astrophys. **594**, A24 (2016).
- [37] S. Bocquet *et al.* (SPT Collaboration), Cluster cosmology constraints from the 2500 deg<sup>2</sup> SPT-SZ survey: Inclusion of weak gravitational lensing data from Magellan and the Hubble Space Telescope, Astrophys. J. **878**, 55 (2019).

- [38] Pierre Zhang, Guido D'Amico, Leonardo Senatore, Cheng Zhao, and Yifu Cai, BOSS correlation function analysis from the effective field theory of large-scale structure, J. Cosmol. Astropart. Phys. 02 (2022) 036.
- [39] Oliver H. E. Philcox and Mikhail M. Ivanov, BOSS DR12 full-shape cosmology: ΛCDM constraints from the largescale galaxy power spectrum and bispectrum monopole, Phys. Rev. D 105, 043517 (2022).
- [40] Guido D'Amico, Yaniv Donath, Matthew Lewandowski, Leonardo Senatore, and Pierre Zhang, The BOSS bispectrum analysis at one loop from the effective field theory of large-scale structure, arXiv:2206.08327.
- [41] Alexandra Amon and George Efstathiou, A non-linear solution to the S<sub>8</sub> tension?, Mon. Not. R. Astron. Soc. **516**, 5355 (2022).
- [42] A. Amon *et al.*, Consistent lensing and clustering in a low-S<sub>8</sub> Universe with BOSS, DES Year 3, HSC Year 1 and KiDS-1000, Mon. Not. R. Astron. Soc. **518**, 477 (2023).
- [43] Jose Luis Bernal, Licia Verde, and Adam G. Riess, The trouble with  $H_0$ , J. Cosmol. Astropart. Phys. 10 (2016) 019
- [44] Kevin Aylor, Mackenzie Joy, Lloyd Knox, Marius Millea, Srinivasan Raghunathan, and W. L. Kimmy Wu, Sounds discordant: Classical distance ladder & ΛCDM-based determinations of the cosmological sound horizon, Astrophys. J. 874, 4 (2019).
- [45] Lloyd Knox and Marius Millea, Hubble constant hunter's guide, Phys. Rev. D 101, 043533 (2020).
- [46] David Camarena and Valerio Marra, On the use of the local prior on the absolute magnitude of type Ia supernovae in cosmological inference, Mon. Not. R. Astron. Soc. **504**, 5164 (2021).
- [47] George Efstathiou, To  $H_0$  or not to  $H_0$ ?, Mon. Not. R. Astron. Soc. **505**, 3866 (2021).
- [48] Nils Schöneberg, Guillermo Franco Abellán, Andrea Pérez Sánchez, Samuel J. Witte, Vivian Poulin, and Julien Lesgourgues, The  $H_0$  olympics: A fair ranking of proposed models, Phys. Rep. **984**, 1 (2022).
- [49] Christina D. Kreisch, Francis-Yan Cyr-Racine, and Olivier Doré, Neutrino puzzle: Anomalies, interactions, and cosmological tensions, Phys. Rev. D 101, 123505 (2020).
- [50] Maximilian Berbig, Sudip Jana, and Andreas Trautner, The Hubble tension and a renormalizable model of gauged neutrino self-interactions, Phys. Rev. D 102, 115008 (2020).
- [51] Subhajit Ghosh, Rishi Khatri, and Tuhin S. Roy, Can dark neutrino interactions phase out the Hubble tension?, Phys. Rev. D 102, 123544 (2020).
- [52] Francesco Forastieri, Massimiliano Lattanzi, and Paolo Natoli, Cosmological constraints on neutrino selfinteractions with a light mediator, Phys. Rev. D 100, 103526 (2019).
- [53] Miguel Escudero and Samuel J. Witte, A CMB search for the neutrino mass mechanism and its relation to the Hubble tension, Eur. Phys. J. C **80**, 294 (2020).
- [54] Miguel Escudero and Samuel J. Witte, The Hubble tension as a hint of leptogenesis and neutrino mass generation, Eur. Phys. J. C 81, 515 (2021).

- [55] Nikita Blinov and Gustavo Marques-Tavares, Interacting radiation after Planck and its implications for the Hubble tension, J. Cosmol. Astropart. Phys. 09 (2020) 029.
- [56] Subhajit Ghosh, Soubhik Kumar, and Yuhsin Tsai, Freestreaming and coupled dark radiation isocurvature perturbations: Constraints and application to the Hubble tension, J. Cosmol. Astropart. Phys. 05 (2022) 014.
- [57] Maria Archidiacono and Stefano Gariazzo, Two sides of the same coin: Sterile neutrinos and dark radiation. Status and perspectives, Universe 8, 175 (2022).
- [58] Daniel Aloni, Asher Berlin, Melissa Joseph, Martin Schmaltz, and Neal Weiner, A step in understanding the Hubble tension, Phys. Rev. D 105, 123516 (2022).
- [59] Nils Schöneberg and Guillermo Franco Abellán, A step in the right direction? Analyzing the Wess Zumino dark radiation solution to the Hubble tension, J. Cosmol. Astropart. Phys. 12 (2022) 001.
- [60] Tanvi Karwal and Marc Kamionkowski, Dark energy at early times, the Hubble parameter, and the string axiverse, Phys. Rev. D 94, 103523 (2016).
- [61] Vivian Poulin, Tristan L. Smith, Tanvi Karwal, and Marc Kamionkowski, Early Dark Energy Can Resolve the Hubble Tension, Phys. Rev. Lett. 122, 221301 (2019).
- [62] Tristan L. Smith, Vivian Poulin, and Mustafa A. Amin, Oscillating scalar fields and the Hubble tension: A resolution with novel signatures, Phys. Rev. D 101, 063523 (2020).
- [63] Florian Niedermann and Martin S. Sloth, New early dark energy, Phys. Rev. D 103, L041303 (2021).
- [64] Florian Niedermann and Martin S. Sloth, Resolving the Hubble tension with new early dark energy, Phys. Rev. D 102, 063527 (2020).
- [65] Gen Ye and Yun-Song Piao, Is the Hubble tension a hint of AdS phase around recombination?, Phys. Rev. D 101, 083507 (2020).
- [66] Janina Renk, Miguel Zumalacárregui, Francesco Montanari, and Alexandre Barreira, Galileon gravity in light of ISW, CMB, BAO and H<sub>0</sub> data, J. Cosmol. Astropart. Phys. 10 (2017) 020.
- [67] C. Umiltà, M. Ballardini, F. Finelli, and D. Paoletti, CMB and BAO constraints for an induced gravity dark energy model with a quartic potential, J. Cosmol. Astropart. Phys. 08 (2015) 017.
- [68] Mario Ballardini, Fabio Finelli, Caterina Umiltà, and Daniela Paoletti, Cosmological constraints on induced gravity dark energy models, J. Cosmol. Astropart. Phys. 05 (2016) 067.
- [69] Massimo Rossi, Mario Ballardini, Matteo Braglia, Fabio Finelli, Daniela Paoletti, Alexei A. Starobinsky, and Caterina Umiltà, Cosmological constraints on post-Newtonian parameters in effectively massless scalar-tensor theories of gravity, Phys. Rev. D 100, 103524 (2019).
- [70] Matteo Braglia, Mario Ballardini, William T. Emond, Fabio Finelli, A. Emir Gumrukcuoglu, Kazuya Koyama, and Daniela Paoletti, Larger value for H<sub>0</sub> by an evolving gravitational constant, Phys. Rev. D 102, 023529 (2020).
- [71] Miguel Zumalacarregui, Gravity in the era of equality: Towards solutions to the Hubble problem without fine-tuned initial conditions, Phys. Rev. D **102**, 023523 (2020).

- [72] Tal Abadi and Ely D. Kovetz, Can conformally coupled modified gravity solve the Hubble tension?, Phys. Rev. D **103**, 023530 (2021).
- [73] Mario Ballardini, Matteo Braglia, Fabio Finelli, Daniela Paoletti, Alexei A. Starobinsky, and Caterina Umiltà, Scalar-tensor theories of gravity, neutrino physics, and the *H*<sub>0</sub> tension, J. Cosmol. Astropart. Phys. 10 (2020) 044.
- [74] Matteo Braglia, William T. Emond, Fabio Finelli, A. Emir Gumrukcuoglu, and Kazuya Koyama, Unified framework for early dark energy from α-attractors, Phys. Rev. D 102, 083513 (2020).
- [75] Eleonora Di Valentino, Alessandro Melchiorri, and Joseph Silk, Cosmological hints of modified gravity?, Phys. Rev. D 93, 023513 (2016).
- [76] Sebastian Bahamonde, Konstantinos F. Dialektopoulos, Celia Escamilla-Rivera, Gabriel Farrugia, Viktor Gakis, Martin Hendry, Manuel Hohmann, Jackson Levi Said, Jurgen Mifsud, and Eleonora Di Valentino, Teleparallel gravity: From theory to cosmology, arXiv:2106.13793.
- [77] Marco Raveri, Reconstructing gravity on cosmological scales, Phys. Rev. D **101**, 083524 (2020).
- [78] Sheng-Feng Yan, Pierre Zhang, Jie-Wen Chen, Xin-Zhe Zhang, Yi-Fu Cai, and Emmanuel N. Saridakis, Interpreting cosmological tensions from the effective field theory of torsional gravity, Phys. Rev. D 101, 121301 (2020).
- [79] Noemi Frusciante, Simone Peirone, Luis Atayde, and Antonio De Felice, Phenomenology of the generalized cubic covariant Galileon model and cosmological bounds, Phys. Rev. D 101, 064001 (2020).
- [80] Joan Solà Peracaula, Adria Gomez-Valent, Javier de Cruz Pérez, and Cristian Moreno-Pulido, Brans-Dicke gravity with a cosmological constant smoothes out ΛCDM tensions, Astrophys. J. Lett. 886, L6 (2019).
- [81] Joan Solà Peracaula, Adrià Gómez-Valent, Javier de Cruz Pérez, and Cristian Moreno-Pulido, Brans-Dicke cosmology with a Λ-term: A possible solution to ΛCDM tensions, Classical Quantum Gravity 37, 245003 (2020).
- [82] Guillermo Ballesteros, Alessio Notari, and Fabrizio Rompineve, The  $H_0$  tension:  $\Delta G_N$  vs.  $\Delta N_{\rm eff}$ , J. Cosmol. Astropart. Phys. 11 (2020) 024.
- [83] Matteo Braglia, Mario Ballardini, Fabio Finelli, and Kazuya Koyama, Early modified gravity in light of the  $H_0$  tension and LSS data, Phys. Rev. D **103**, 043528 (2021).
- [84] Harry Desmond, Bhuvnesh Jain, and Jeremy Sakstein, Local resolution of the Hubble tension: The impact of screened fifth forces on the cosmic distance ladder, Phys. Rev. D 100, 043537 (2019); 101, 069904(E) (2020); 101, 129901(E) (2020).
- [85] Meng-Xiang Lin, Marco Raveri, and Wayne Hu, Phenomenology of modified gravity at recombination, Phys. Rev. D 99, 043514 (2019).
- [86] Chi-Ting Chiang and Anže Slosar, Inferences of  $H_0$  in presence of a non-standard recombination, arXiv: 1811.03624.
- [87] Luke Hart and Jens Chluba, Updated fundamental constant constraints from Planck 2018 data and possible relations to the Hubble tension, Mon. Not. R. Astron. Soc. 493, 3255 (2020).

- [88] Toyokazu Sekiguchi and Tomo Takahashi, Early recombination as a solution to the  $H_0$  tension, Phys. Rev. D **103**, 083507 (2021).
- [89] Karsten Jedamzik and Levon Pogosian, Relieving the Hubble Tension with Primordial Magnetic Fields, Phys. Rev. Lett. **125**, 181302 (2020).
- [90] Francis-Yan Cyr-Racine, Fei Ge, and Lloyd Knox, A Symmetry of Cosmological Observables, and a High Hubble Constant as an Indicator of a Mirror World Dark Sector, Phys. Rev. Lett. 128, 201301 (2022).
- [91] Shadab Alam *et al.* (BOSS Collaboration), The clustering of galaxies in the completed SDSS-III Baryon Oscillation Spectroscopic Survey: Cosmological analysis of the DR12 galaxy sample, Mon. Not. R. Astron. Soc. **470**, 2617 (2017).
- [92] Daniel Baumann, Alberto Nicolis, Leonardo Senatore, and Matias Zaldarriaga, Cosmological non-linearities as an effective fluid, J. Cosmol. Astropart. Phys. 07 (2012) 051.
- [93] John Joseph M. Carrasco, Mark P. Hertzberg, and Leonardo Senatore, The effective field theory of cosmological large scale structures, J. High Energy Phys. 09 (2012) 082.
- [94] Leonardo Senatore and Matias Zaldarriaga, The IRresummed effective field theory of large scale structures, J. Cosmol. Astropart. Phys. 02 (2015) 013.
- [95] Leonardo Senatore, Bias in the effective field theory of large scale structures, J. Cosmol. Astropart. Phys. 11 (2015) 007.
- [96] Leonardo Senatore and Matias Zaldarriaga, Redshift space distortions in the effective field theory of large scale structures, arXiv:1409.1225.
- [97] Ashley Perko, Leonardo Senatore, Elise Jennings, and Risa H. Wechsler, Biased tracers in redshift space in the EFT of large-scale structure, arXiv:1610.09321.
- [98] Guido D'Amico, Jérôme Gleyzes, Nickolas Kokron, Dida Markovic, Leonardo Senatore, Pierre Zhang, Florian Beutler, and Héctor Gil-Marín, The cosmological analysis of the SDSS/BOSS data from the effective field theory of large-scale structure, J. Cosmol. Astropart. Phys. 05 (2020) 005.
- [99] Mikhail M. Ivanov, Marko Simonović, and Matias Zaldarriaga, Cosmological parameters from the BOSS galaxy power spectrum, J. Cosmol. Astropart. Phys. 05 (2020) 042.
- [100] Thomas Colas, Guido D'amico, Leonardo Senatore, Pierre Zhang, and Florian Beutler, Efficient cosmological analysis of the SDSS/BOSS data from the effective field theory of large-scale structure, J. Cosmol. Astropart. Phys. 06 (2020) 001.
- [101] Guido D'Amico, Leonardo Senatore, and Pierre Zhang, Limits on wCDM from the EFTofLSS with the PyBird code, J. Cosmol. Astropart. Phys. 01 (2021) 006.
- [102] Guido D'Amico, Yaniv Donath, Leonardo Senatore, and Pierre Zhang, Limits on clustering and smooth quintessence from the EFTofLSS, arXiv:2012.07554.
- [103] Théo Simon, Guillermo Franco Abellán, Peizhi Du, Vivian Poulin, and Yuhsin Tsai, Constraining decaying dark matter with BOSS data and the effective field theory of large-scale structures, Phys. Rev. D 106, 023516 (2022).

- [104] Shi-Fan Chen, Zvonimir Vlah, and Martin White, A new analysis of galaxy 2-point functions in the BOSS survey, including full-shape information and post-reconstruction BAO, J. Cosmol. Astropart. Phys. 02 (2022) 008.
- [105] Suresh Kumar, Rafael C. Nunes, and Priya Yadav, Updating non-standard neutrinos properties with Planck-CMB data and full-shape analysis of BOSS and eBOSS galaxies, J. Cosmol. Astropart. Phys. 09 (2022) 060.
- [106] Rafael C. Nunes, Sunny Vagnozzi, Suresh Kumar, Eleonora Di Valentino, and Olga Mena, New tests of dark sector interactions from the full-shape galaxy power spectrum, Phys. Rev. D 105, 123506 (2022).
- [107] Alex Laguë, J. Richard Bond, Renée Hložek, Keir K. Rogers, David J. E. Marsh, and Daniel Grin, Constraining ultralight axions with galaxy surveys, J. Cosmol. Astropart. Phys. 01 (2022) 049.
- [108] Théo Simon, Pierre Zhang, Vivian Poulin, and Tristan L. Smith, On the consistency of effective field theory analyses of BOSS power spectrum, arXiv:2208.05929.
- [109] Meng-Xiang Lin, Giampaolo Benevento, Wayne Hu, and Marco Raveri, Acoustic dark energy: Potential conversion of the Hubble tension, Phys. Rev. D 100, 063542 (2019).
- [110] Kim V. Berghaus and Tanvi Karwal, Thermal friction as a solution to the Hubble tension, Phys. Rev. D 101, 083537 (2020).
- [111] Tanvi Karwal, Marco Raveri, Bhuvnesh Jain, Justin Khoury, and Mark Trodden, Chameleon early dark energy and the Hubble tension, Phys. Rev. D **105**, 063535 (2022).
- [112] J. Colin Hill *et al.*, The Atacama Cosmology Telescope: Constraints on pre-recombination early dark energy, Phys. Rev. D **105**, 123536 (2022).
- [113] Vivian Poulin, Tristan L. Smith, and Alexa Bartlett, Dark energy at early times and ACT: A larger Hubble constant without late-time priors, Phys. Rev. D 104, 123550 (2021).
- [114] Adrien La Posta, Thibaut Louis, Xavier Garrido, and J. Colin Hill, Constraints on pre-recombination early dark energy from SPT-3G public data, Phys. Rev. D 105, 083519 (2022).
- [115] Tristan L. Smith, Matteo Lucca, Vivian Poulin, Guillermo F. Abellan, Lennart Balkenhol, Karim Benabed, Silvia Galli, and Riccardo Murgia, Hints of early dark energy in Planck, SPT, and ACT data: New physics or systematics?, Phys. Rev. D 106, 043526 (2022).
- [116] J. Colin Hill, Evan McDonough, Michael W. Toomey, and Stephon Alexander, Early dark energy does not restore cosmological concordance, Phys. Rev. D **102**, 043507 (2020).
- [117] Sunny Vagnozzi, Consistency tests of ΛCDM from the early ISW effect: Implications for early-time new physics and the Hubble tension, Phys. Rev. D **104**, 063524 (2021).
- [118] Mikhail M. Ivanov, Evan McDonough, J. Colin Hill, Marko Simonović, Michael W. Toomey, Stephon Alexander, and Matias Zaldarriaga, Constraining early dark energy with large-scale structure, Phys. Rev. D 102, 103502 (2020).
- [119] Guido D'Amico, Leonardo Senatore, Pierre Zhang, and Henry Zheng, The Hubble tension in light of the full-shape analysis of large-scale structure data, J. Cosmol. Astropart. Phys. 05 (2021) 072.

- [120] Tristan L. Smith, Vivian Poulin, José Luis Bernal, Kimberly K. Boddy, Marc Kamionkowski, and Riccardo Murgia, Early dark energy is not excluded by current large-scale structure data, Phys. Rev. D 103, 123542 (2021).
- [121] Riccardo Murgia, Guillermo F. Abellán, and Vivian Poulin, Early dark energy resolution to the Hubble tension in light of weak lensing surveys and lensing anomalies, Phys. Rev. D **103**, 063502 (2021).
- [122] Adrià Gómez-Valent, A fast test to assess the impact of marginalization in Monte Carlo analyses, and its application to cosmology, Phys. Rev. D **106**, 063506 (2022).
- [123] Laura Herold, Elisa G. M. Ferreira, and Eiichiro Komatsu, New constraint on early dark energy from Planck and BOSS data using the profile likelihood, Astrophys. J. Lett. 929, L16 (2022).
- [124] Alexander Reeves, Laura Herold, Sunny Vagnozzi, Blake D. Sherwin, and Elisa G. M. Ferreira, Restoring cosmological concordance with early dark energy and massive neutrinos?, arXiv:2207.01501.
- [125] Florian Niedermann and Martin S. Sloth, New early dark energy is compatible with current LSS data, Phys. Rev. D 103, 103537 (2021).
- [126] Oliver H. E. Philcox, Gerrit S. Farren, Blake D. Sherwin, Eric J. Baxter, and Dillon J. Brout, Determining the Hubble constant without the sound horizon: A 3.6% constraint on  $H_0$  from galaxy surveys, CMB lensing and supernovae, Phys. Rev. D **106**, 063530 (2022).
- [127] Dillon Brout *et al.*, The Pantheon+ analysis: Cosmological constraints, Astrophys. J. **938**, 110 (2022).
- [128] Michael S. Turner, Coherent scalar-field oscillations in an expanding universe, Phys. Rev. D 28, 1243 (1983).
- [129] Vivian Poulin, Tristan L. Smith, Daniel Grin, Tanvi Karwal, and Marc Kamionkowski, Cosmological implications of ultralight axionlike fields, Phys. Rev. D 98, 083525 (2018).
- [130] Karsten Jedamzik, Levon Pogosian, and Gong-Bo Zhao, Why reducing the cosmic sound horizon alone can not fully resolve the Hubble tension, Commun. Phys. **4**, 123 (2021).
- [131] Benjamin Audren, Julien Lesgourgues, Karim Benabed, and Simon Prunet, Conservative constraints on early cosmology: An illustration of the Monte Python cosmological parameter inference code, J. Cosmol. Astropart. Phys. 02 (2013) 001.
- [132] Thejs Brinckmann and Julien Lesgourgues, MONTE PYTHON 3: Boosted MCMC sampler and other features, Phys. Dark Universe **24**, 100260 (2019).
- [133] Diego Blas, Julien Lesgourgues, and Thomas Tram, The Cosmic Linear Anisotropy Solving System (CLASS) II: Approximation schemes, J. Cosmol. Astropart. Phys. 07 (2011) 034.
- [134] N. Aghanim *et al.* (Planck Collaboration), Planck 2018 results. VIII. Gravitational lensing, Astron. Astrophys. **641**, A8 (2020).
- [135] Steve K. Choi *et al.* (ACT Collaboration), The Atacama Cosmology Telescope: A measurement of the cosmic microwave background power spectra at 98 and 150 GHz, J. Cosmol. Astropart. Phys. 12 (2020) 045.

- [136] Nils Schöneberg, Julien Lesgourgues, and Deanna C. Hooper, The BAO + BBN take on the Hubble tension, J. Cosmol. Astropart. Phys. 10 (2019) 029.
- [137] R. Consiglio, P. F. de Salas, G. Mangano, G. Miele, S. Pastor, and O. Pisanti, PArthENoPE reloaded, Comput. Phys. Commun. 233, 237 (2018).
- [138] Ryan J. Cooke, Max Pettini, and Charles C. Steidel, One percent determination of the primordial deuterium abundance, Astrophys. J. 855, 102 (2018).
- [139] Erik Aver, Keith A. Olive, and Evan D. Skillman, The effects of He I λ10830 on helium abundance determinations, J. Cosmol. Astropart. Phys. 07 (2015) 011.
- [140] Florian Beutler, Chris Blake, Matthew Colless, D. Heath Jones, Lister Staveley-Smith, Lachlan Campbell, Quentin Parker, Will Saunders, and Fred Watson, The 6dF galaxy survey: Baryon acoustic oscillations and the local Hubble constant, Mon. Not. R. Astron. Soc. 416, 3017 (2011).
- [141] Ashley J. Ross, Lado Samushia, Cullan Howlett, Will J. Percival, Angela Burden, and Marc Manera, The clustering of the SDSS DR7 main galaxy sample—I. A 4 per cent distance measure at z=0.15, Mon. Not. R. Astron. Soc. **449**, 835 (2015).
- [142] Héctor Gil-Marín et al., The clustering of galaxies in the SDSS-III Baryon Oscillation Spectroscopic Survey: BAO measurement from the LOS-dependent power spectrum of DR12 BOSS galaxies, Mon. Not. R. Astron. Soc. 460, 4210 (2016).
- [143] Francisco-Shu Kitaura *et al.*, The clustering of galaxies in the SDSS-III Baryon Oscillation Spectroscopic Survey: Mock galaxy catalogues for the BOSS final data release, Mon. Not. R. Astron. Soc. **456**, 4156 (2016).
- [144] Beth Reid *et al.*, SDSS-III Baryon Oscillation Spectroscopic Survey Data Release 12: Galaxy target selection and large scale structure catalogues, Mon. Not. R. Astron. Soc. **455**, 1553 (2016).
- [145] D. M. Scolnic *et al.*, The complete light-curve sample of spectroscopically confirmed SNe Ia from Pan-STARRS1 and cosmological constraints from the combined Pantheon sample, Astrophys. J. 859, 101 (2018).
- [146] Antony Lewis, GetDist: A PYTHON package for analysing Monte Carlo samples, arXiv:1910.13970.
- [147] Héctor Gil-Marín et al., The clustering of galaxies in the SDSS-III Baryon Oscillation Spectroscopic Survey: RSD measurement from the LOS-dependent power spectrum of DR12 BOSS galaxies, Mon. Not. R. Astron. Soc. 460, 4188 (2016).
- [148] Cheng Zhao *et al.*, The completed SDSS-IV extended Baryon Oscillation Spectroscopic Survey: 1000 multi-tracer mock catalogues with redshift evolution and systematics for galaxies and quasars of the final data release, Mon. Not. R. Astron. Soc. **503**, 1149 (2021).
- [149] Nick Hand, Yu Feng, Florian Beutler, Yin Li, Chirag Modi, Uros Seljak, and Zachary Slepian, NBODYKIT: An open-source, massively parallel toolkit for large-scale structure, Astron. J. **156**, 160 (2018).
- [150] Florian Beutler and Patrick McDonald, Unified galaxy power spectrum measurements from 6dFGS, BOSS, and eBOSS, J. Cosmol. Astropart. Phys. 11 (2021) 031.

- [151] Oliver H. E. Philcox, Cosmology without window functions: Quadratic estimators for the galaxy power spectrum, Phys. Rev. D 103, 103504 (2021).
- [152] Florian Beutler *et al.* (BOSS Collaboration), The clustering of galaxies in the completed SDSS-III Baryon Oscillation Spectroscopic Survey: Baryon acoustic oscillations in the Fourier space, Mon. Not. R. Astron. Soc. **464**, 3409 (2017).
- [153] Oliver H. E. Philcox, Mikhail M. Ivanov, Marko Simonović, and Matias Zaldarriaga, Combining full-shape and BAO analyses of galaxy power spectra: A 1.6% CMB-independent constraint on H<sub>0</sub>, J. Cosmol. Astropart. Phys. 05 (2020) 032.
- [154] Anton Chudaykin, Mikhail M. Ivanov, Oliver H. E. Philcox, and Marko Simonović, Nonlinear perturbation theory extension of the Boltzmann code CLASS, Phys. Rev. D 102, 063533 (2020).
- [155] Diego Blas, Mathias Garny, Mikhail M. Ivanov, and Sergey Sibiryakov, Time-sliced perturbation theory II: Baryon acoustic oscillations and infrared resummation, J. Cosmol. Astropart. Phys. 07 (2016) 028.
- [156] Mikhail M. Ivanov and Sergey Sibiryakov, Infrared resummation for biased tracers in redshift space, J. Cosmol. Astropart. Phys. 07 (2018) 053.
- [157] Matthew Lewandowski, Leonardo Senatore, Francisco Prada, Cheng Zhao, and Chia-Hsun Chuang, EFT of large scale structures in redshift space, Phys. Rev. D 97, 063526 (2018).
- [158] Matthew Lewandowski and Leonardo Senatore, An analytic implementation of the IR-resummation for the BAO peak, J. Cosmol. Astropart. Phys. 03 (2020) 018.
- [159] Marco Raveri and Wayne Hu, Concordance and discordance in cosmology, Phys. Rev. D **99**, 043506 (2019).
- [160] Evan McDonough, Meng-Xiang Lin, J. Colin Hill, Wayne Hu, and Shengjia Zhou, The early dark sector, the Hubble tension, and the swampland, Phys. Rev. D **106**, 043525 (2022).
- [161] Vivian I. Sabla and Robert R. Caldwell, The microphysics of early dark energy, Phys. Rev. D 106, 063526 (2022).
- [162] Itamar J. Allali, Mark P. Hertzberg, and Fabrizio Rompineve, Dark sector to restore cosmological concordance, Phys. Rev. D 104, L081303 (2021).
- [163] Steven J. Clark, Kyriakos Vattis, JiJi Fan, and Savvas M. Koushiappas, The  $H_0$  and  $S_8$  tensions necessitate early and late time changes to  $\Lambda$ CDM, arXiv:2110.09562.
- [164] Guido D'Amico, Matthew Lewandowski, Leonardo Senatore, and Pierre Zhang, Limits on primordial non-Gaussianities from BOSS galaxy-clustering data, arXiv: 2201.11518.
- [165] Shadab Alam et al. (eBOSS Collaboration), Completed SDSS-IV extended Baryon Oscillation Spectroscopic Survey: Cosmological implications from two decades of spectroscopic surveys at the Apache Point Observatory, Phys. Rev. D 103, 083533 (2021).
- [166] José Luis Bernal, Licia Verde, Raul Jimenez, Marc Kamionkowski, David Valcin, and Benjamin D. Wandelt, The trouble beyond  $H_0$  and the new cosmic triangles, Phys. Rev. D **103**, 103533 (2021).
- [167] Michael Boylan-Kolchin and Daniel R. Weisz, Uncertain times: The redshift-time relation from cosmology and stars, Mon. Not. R. Astron. Soc. 505, 2764 (2021).

- [168] Anatoly Klypin, Vivian Poulin, Francisco Prada, Joel Primack, Marc Kamionkowski, Vladimir Avila-Reese, Aldo Rodriguez-Puebla, Peter Behroozi, Doug Hellinger, and Tristan L. Smith, Clustering and halo abundances in early dark energy cosmological models, Mon. Not. R. Astron. Soc. 504, 769 (2021).
- [169] Michael Boylan-Kolchin, Stress testing ΛCDM with highredshift galaxy candidates, arXiv:2208.01611.
- [170] Guido D'Amico, Nemanja Kaloper, and Alexander Westphal, General double monodromy inflation, Phys. Rev. D 105, 103527 (2022).
- [171] Renata Kallosh and Andrei Linde, Hybrid cosmological attractors, Phys. Rev. D 106, 023522 (2022).
- [172] Jun-Qian Jiang and Yun-Song Piao, Towards early dark energy and  $n_s = 1$  with Planck, ACT and SPT, Phys. Rev. D **105**, 103514 (2022).
- [173] Fuminobu Takahashi and Wen Yin, Cosmological implications of  $n_s \approx 1$  in light of the Hubble tension, Phys. Lett. B **830**, 137143 (2022).
- [174] Arnaud de Mattia and Vanina Ruhlmann-Kleider, Integral constraints in spectroscopic surveys, J. Cosmol. Astropart. Phys. 08 (2019) 036.
- [175] Arnaud de Mattia *et al.*, The completed SDSS-IV extended Baryon Oscillation Spectroscopic Survey: Measurement of the BAO and growth rate of structure of the emission line galaxy sample from the anisotropic power spectrum between redshift 0.6 and 1.1, Mon. Not. R. Astron. Soc. **501**, 5616 (2021).
- [176] Naonori S. Sugiyama, Shun Saito, Florian Beutler, and Hee-Jong Seo, A complete FFT-based decomposition

- formalism for the redshift-space bispectrum, Mon. Not. R. Astron. Soc. **484**, 364 (2019).
- [177] Hume A. Feldman, Nick Kaiser, and John A. Peacock, Power spectrum analysis of three-dimensional redshift surveys, Astrophys. J. 426, 23 (1994).
- [178] Kazuhiro Yamamoto, Optimal weighting scheme in redshift space power spectrum analysis and a prospect for measuring the cosmic equation of state, Astrophys. J. 595, 577 (2003).
- [179] Kazuhiro Yamamoto, Masashi Nakamichi, Akinari Kamino, Bruce A. Bassett, and Hiroaki Nishioka, A measurement of the quadrupole power spectrum in the clustering of the 2dF QSO Survey, Publ. Astron. Soc. Jpn. 58, 93 (2006).
- [180] Davide Bianchi, Héctor Gil-Marín, Rossana Ruggeri, and Will J. Percival, Measuring line-of-sight dependent Fourier-space clustering using FFTs, Mon. Not. R. Astron. Soc. 453, L11 (2015).
- [181] Roman Scoccimarro, Fast estimators for redshift-space clustering, Phys. Rev. D 92, 083532 (2015).
- [182] Florian Beutler, Emanuele Castorina, and Pierre Zhang, Interpreting measurements of the anisotropic galaxy power spectrum, J. Cosmol. Astropart. Phys. 03 (2019) 040.
- [183] Pierre Zhang and Yifu Cai, BOSS full-shape analysis from the EFTofLSS with exact time dependence, J. Cosmol. Astropart. Phys. 01 (2022) 031.
- [184] Florian Beutler *et al.* (BOSS Collaboration), The clustering of galaxies in the completed SDSS-III Baryon Oscillation Spectroscopic Survey: Anisotropic galaxy clustering in Fourier-space, Mon. Not. R. Astron. Soc. **466**, 2242 (2017).